INVESTIGATION OF ION-ION RECOMBINATION CROSS SECTIONS

D. L. Huestis, et al

Stanford Research Institute

Prepared for:

Air Force Cambridge Research Laboratories

19 November 1975

AFCRL-TR-75-0606

INVESTIGATION OF ION-ION RECOMBINATION CROSS SECTIONS

D. L. Huestis
J. T. Moseley
D. Mukherjee
J. R. Peterson
F. T. Smith
H. D. Zeman
Stanford Research Institute
Molecular Physics Center
Menlo Park, California 94025

19 November 1975

Scientific Report No.1

SRI Project PYU-3784
MP No.75-73

Approved for public release; distribution unlimited.

This research was sponsored by the Defense Nuclear Agency under subtask S99QAXHD010 Reaction Rates Critical to Propagation, Work Unit 65, entitled "Measurements of Rate Coefficients for Two-Body Positive Ion-Negative Ion Neutralization Reactions" and under subtask S99QAXHD028 Theoretical Studies of Ionizing Mechanisms in the Upper Atmosphere, Work Unit 32, entitled "Theoretical Aspects of the SRI Ion-Ion Laboratory Measurements."

Prepared for
AIR FORCE CAMBRIDGE RESEARCH LABORATORIES
AIR FORCE SYSTEMS COMMAND
UNITED STATES AIR FORCE
HANSCOM AFB, MASSACHUSETTS 01731

Unclassified

SECURITY CLASSIFICATION OF THIS PAGE (When Data Entered)

REPORT DOCUMENTATION PAGE

READ INSTRUCTIONS BEFORE COMPLETING FORM

1. REPORT NUMBER: AFCRL-TR-75-0606

2. GOVT ACCESSION NO.:

3. RECIPIENT'S CATALOG NUMBER:

4. TITLE (and Subtitle): INVESTIGATION OF ION-ION RECOMBINATION CROSS SECTIONS

5. TYPE OF REPORT & PERIOD COVERED: Scientific Report No. 1, 19 Oct. 1974 to 18 Oct 1975

6. PERFORMING ORG. REPORT NUMBER: MP 75-73

7. AUTHOR(s): D. L. Huestis, J. T. Moseley, D. Mukherjee, J. R. Peterson, F. T. Smith and H. D. Zeman

8. CONTRACT OR GRANT NUMBER(s): F19628-75-C-0050

9. PERFORMING ORGANIZATION NAME AND ADDRESS:
Stanford Research Institute
Molecular Physics Center
Menlo Park, California 94025

10. PROGRAM ELEMENT, PROJECT, TASK AREA & WORK UNIT NUMBERS: CDNAOO

11. CONTROLLING OFFICE NAME AND ADDRESS:
Air Force Cambridge Research Laboratories (LKB)
Hanscom AFB, Massachusetts 01731
Contract Monitor: John F. Paulson/LKB

12. REPORT DATE: 19 November 1975

13. NO. OF PAGES: 76

14. MONITORING AGENCY NAME & ADDRESS (if diff. from Controlling Office):

15. SECURITY CLASS. (of this report): Unclassified

15a. DECLASSIFICATION/DOWNGRADING SCHEDULE:

16. DISTRIBUTION STATEMENT (of this report)

Approved for public release; distribution unlimited.

17. DISTRIBUTION STATEMENT (of the abstract entered in Block 20, if different from report)

18. SUPPLEMENTARY NOTES: This research was sponsored by the Defense Nuclear Agency under subtask S99QAXHD019 Reaction Rates Critical to Propagation, Work Unit 65, entitled "Measurements of Rate Coefficients for Two-Body Positive Ion-Negative Ion Neutralization Reactions and under subtask S99QAXHD028 Theoretical Studies of Ionizing Mechanisms in the Upper Atmosphere, Work Unit 32, entitled "Theoretical Aspects of the SRI Ion-Ion Laboratory Measurements.

19. KEY WORDS (Continue on reverse side if necessary and identify by block number)

two-body ion-ion neutralization
merged beams
neutralization reaction rate
electron transfer
hydrated ions
orbital capture
tidal distortion
semiclassical scattering theory

20. ABSTRACT (Continue on reverse side if necessary and identify by block number)

An experimental and theoretical investigation has been made of ion-ion mutual neutralization processes relevant to the chemistry of the D-region of the earth's ionosphere. This work is a continuation of earlier studies under Contract F19628-72-C-0121. In experimental work, the primary effort has been directed toward modifying the merged-beam apparatus, which had been designed to produce beams of small ions, so that it would produce hydrated ion beams of sufficiently high intensity and narrow energy spread. In the theoretical effort,

DD FORM 1 JAN 73 1473

EDITION OF 1 NOV 65 IS OBSOLETE

Unclassified

SECURITY CLASSIFICATION OF THIS PAGE (When Data Entered)

our study of the ion-charged dipole interaction problem, which is being used as a model for the more complex interaction involving two clustered ions, has been continued. A classical dynamical study of this system in two dimensions using a fixed parabolic trajectory approximation and also a less accurate perturbation approximation has been completed. In order to extend this work to the case of three-dimensional motion, a powerful semiclassical perturbation technique, in which the collision S-matrix is expressible in closed form in terms of tabulated functions, has been developed. Using this approach preliminary calculations of orbital capture cross sections for the $O^- + NO^+$ system have been carried out. The uniform semiclassical S-matrix approach enables quantum effects such as interference and tuneling into classically nonallowed regions to be fully accounted for and comparison of semiclassical perturbation results with quantum mechanical close-coupling calculations for the e + CsF system has shown excellent agreement at all but the few smallest quantum numbers. A detailed study of the $NO_2^- \cdot H_2O$ system has been initiated in an effort to extend our approach from rotational excitation of diatomic molecules to the excitation of bending modes in simple hydrated ions.

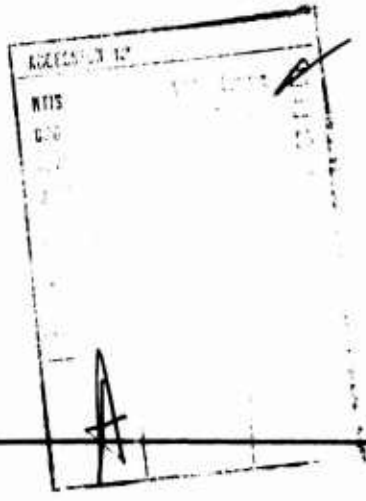

CONTENTS

	Page
LIST OF ILLUSTRATIONS	iv
INTRODUCTION	1
EXPERIMENTAL RESEARCH	3
THEORETICAL RESEARCH	4
Ion-Dipole Ion Scattering Theory	4
Related Work	8
Discussion of the Effect of Clustering on Ion Stability and Neutralization Rates	11
REFERENCES	17
APPENDICES	
A SEMICLASSICAL PERTURBATION SCATTERING BY A RIGID DIPOLE	19
B ELECTRON LOSS CROSS SECTIONS FOR O^-, O_2^-, and NO_3^- IN SEVERAL GASES	23
C ION - ION MUTUAL NEUTRALIZATION	29

LIST OF ILLUSTRATIONS

		Page
1.	Rotor Angular Velocity Versus Incident Ion Position, Strong Interaction Case	5
2.	Structures, $NO_2^-.H_2O = H_2NO_3^-$ (Mass=64)	15

INTRODUCTION

This Annual Scientific Report covers work performed under Contract No. F19628-75-C-0050; previous related contracts were F19628-72-C-0121, AF19(628)-5187, and F19628-69-C-0119.

The work comprises experimental and theoretical determinations of cross sections and reaction rates for the mutual neutralization of positive and negative ions of the type

$$A^+ + B^- \rightarrow A + B \ .$$

These reactions play an important role in determining the ion density and composition in the D-region of the earth's ionosphere. This reaction, along with photodetachment, photodissociation, and positive ion-electron recombination, terminates the chain of events following the initial photoionization of the earth's atmosphere between about 60 and 95 km. The reaction is also important at lower altitudes when the atmosphere is disturbed, such as in the ionization surrounding a nuclear explosion.

Most of the neutralization reactions between simple atmospheric ions were studied quite successfully under previous contracts. Experimental measurements were supplemented by theoretical calculations (without contract support) which led to a fairly good understanding of the reaction mechanisms. More recently, however, the ionospheric problems have centered on reactions between water-clustered ions of the type $NO^+.(H_2O)_n$, $H^+.(H_2O)_n$, $CO_3^-.(H_2O)_n$, and $NO_3^-.(H_2O)_n$, where n is usually between 1 and about 4. These ions are formed slowly by three-body association reactions and dominate the quiescent night-time D region, and probably prevail both day and night at altitudes below

50 km. Because of the slow rates of their formation, and the weakness of the cluster bond (about 1/2 eV), these ions are very difficult to form in beams such as are required by our merging-beam apparatus. Because we anticipated experimental difficulties and delays, and because there were some important physical differences between the neutralization reactions with clustered ions and with the more simple ions, we allocated a significant amount of our contractual effort toward theory. This effort has yielded important insights into the reaction mechanisms, and is approaching the capability of actual cross section and rate calculations.

The current state of the work is described below. In addition, we are submitting three journal reprints as part of this report. One[1] relates directly to the current work, and the others[2-3] concern work performed under previous contracts, but were published during this contract period.

EXPERIMENTAL RESEARCH

The experimental effort has been directed primarily toward improvements to and testing of the apparatus. Several ion source configurations that showed promise for cluster-ion production have been tried. Toward the end of the last contract, a low temperature hollow cathode glow discharge was studied. It produced hydrated ion currents of small but promising magnitudes. Under this contract it was found that the energy spreads in the negative ion beams from this source were prohibitively large and prevented the achievement of sufficient quality in the beams. Analysis of the ion optics in the apparatus also showed several weaknesses that decreased the signal/noise characteristics.

Improvements were undertaken under this contract along three basic lines. Firstly, to produce hydrated ion beams of reasonably high intensity and narrow energy spread, we built and tested hollow cathode duoplasmatron sources. The low currents of hydrated ion beams produced even by these highly efficient sources required an improvement in the sensitivity of the apparatus. For this second goal, we made changes in the ion optical system to improve the ion beam quality, the exactness with which the ion beams are merged and demerged, and the sensitivity with which the neutral beam can be detected. Thirdly, the vacuum system was reorganized and poor components were repaired or replaced in order to improve the vacuum attained as well as to increase ease of operation and to decrease the chance of a catastrophic vacuum failure through the use of various automatic vacuum safety devices.

THEORETICAL RESEARCH

Ion-Dipole Ion Scattering Theory

During the first year of this contract we have continued the theoretical study of the mechanism of recombination of hydrated or clustered ions in the ionosphere that was begun under the preceding contract period.[4] To date we have focused our attention on the interaction of an atomic ion with a rigid dipolar ion as a model problem for developing and testing approximation techniques to be applied to the more complex situation involving clustered ions.

In the initial phase of this effort we studied the ion-dipolar ion problem in two dimensions. Using the efficient and rapid computing scheme that we developed earlier for integrating the fixed parabolic orbit classical equations of motion, we have carried out a systematic investigation of the trajectories to determine the preferential conditions leading to energy transfer and orbital trapping. We have found that the trajectories can be characterized by the number of times the rotor reverses direction as the ion goes by, this number depending on such orbit parameters as the distance of closest approach, the relative phase of the rotor's motion, and the initial rotor energy. As the conditions for rotor reversal are approached, large energy transfer becomes possible. The capture cross section depends on the relative amount of phase space associated with the transitions giving large energy transfer. Figure 1 shows the typical results under conditions of strong interaction between the ion and the charged dipole. Here, the rotor's reduced angular velocity (omega) has been plotted versus the angular position of the ion (phi = - π initially and = 0 at the turning point of the trajectory) for a wide range of initial rotor phases, all other initial conditions remaining constant.

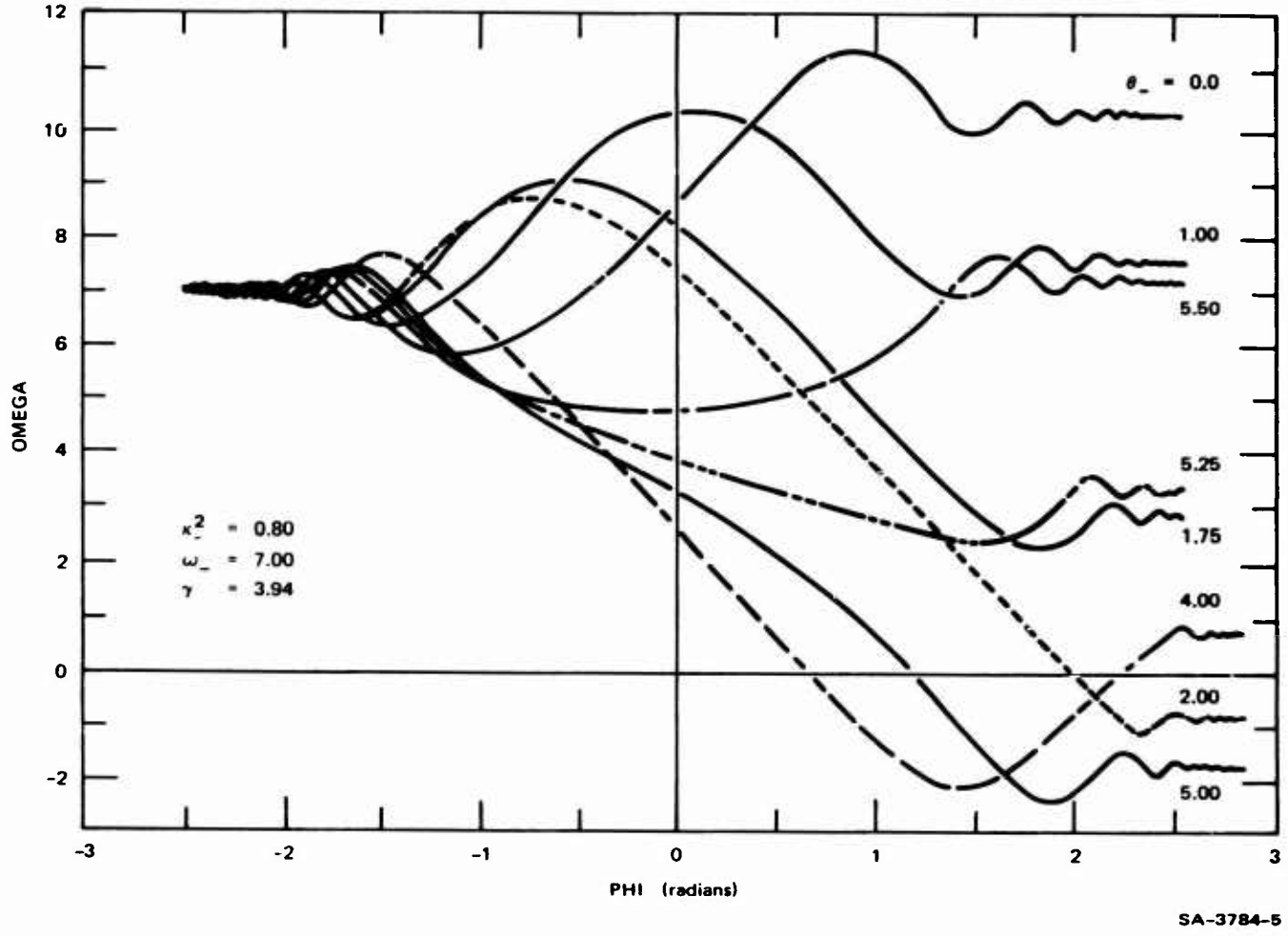

FIGURE 1 ROTOR ANGULAR VELOCITY VERSUS INCIDENT ION POSITION, (STRONG INTERACTION CASE)

We have carried out a systematic comparison of these fixed orbit numerical calculation results with those obtained from a first order perturbation solution of the equations of motion in which the rotational energy transfer is expressible in closed form in terms of Airy functions and their derivatives. These comparisons suggest that the simple perturbation approach is a reasonably good first approximation to the maximum energy transfer available under given conditions. These results were reported by Dr. Felix T. Smith in a paper contributed to the meeting of the Division of Electron and Atomic Physics of the American Physical Society in Chicago, December 2-4, 1974.

Following the development of satisfactory techniques for treating the two-dimensional ion-dipolar ion problem, we turned our attention to extending the number of degrees of freedom that we could handle. To begin with, we concentrated on the extension from motion in a plane to motion in three-dimensional space, which, for our problem, brings in two additional degrees of freedom. We initially based this extension on the analogous work of R. J. Cross, and in this context we reviewed and extended his work in connection with the interaction of an ion with a neutral dipole.[5] His perturbation theory approach is closely analogous to the one we have been using except that the problem of the neutral dipole involves trajectories that are straight lines instead of parabolic, with the result that the Bessel functions K_0 and K_1 appear instead of the Airy functions that are appropriate to the coulomb problem. To determine the capture probability, which is a function of the initial relative kinetic energy, initial dipole rotational energy, and the impact parameter, it is necessary to carry out an averaging procedure over the three angles (specifying the orientation of the rotor's position and angular velocity at some reference point) appearing in the expression for the rotational energy transfer.

Unfortunately, we have found that the necessary averaging procedure, though possible in principle, would require an excessive computational effort.

To avoid this difficulty we reexamined the problem, making maximum use of a representation in angular momentum rather than angular coordinates so as to take advantage of angular momentum conservation laws. In this context we have been able to make use of the work of Miller,[6,7] whose approach leads to a considerable simplification of the problem and allows treatment of the full three-dimensional motion with an apparatus that is hardly more complicated than is needed for the two-dimensional problem. We made use of the first-order classical perturbation treatment that led to an expression in terms of Airy functions in the two-dimensional case and, as it turned out, exactly the same integrals suffice for the new three-dimensional expressions. The perturbation theory, when applied semiclassically, gives us a convenient closed-form expression for the full scattering matrix, and Professor Miller assisted us in extending this, using a uniform approximation to cover quantum effects in the nonclassical region of the motion. The only limitations of this procedure apply in very close encounters when the interaction forces are so great that first order perturbation theory ceases to be appropriate. We feel that these will be for very small classical impact parameters and ordinarily will not contribute much to the cross sections of interest. In any case, they can be treated through the use of classical trajectory calculations for which we have already developed good computing programs.

A paper describing our semiclassical perturbation technique was published in the October 20, 1975 issue of Physical Review Letters.[1] A copy of that article is included as Appendix A of this report. Furthermore, details of the new semiclassical technique and some preliminary results on the cross sections for capture of O^- by NO^+ were

presented by Dr. Felix T. Smith in a contributed paper at the IXth International Conference on the Physics of Electronic and Atomic Collisions held at the University of Washington in Seattle, Washington, July 24-30, 1975.

Since that meeting, considerable effort has been devoted to improving and checking the computing schemes for evaluating the capture cross sections starting from the perturbation semiclassical form of the S-matrix. Thus we are now in a position to generate in a systematic fashion further capture cross sections for reactions of the type $A^- + BC^+$ where the molecular ion has varying dipole moment and varying moment of inertia.

Related Work

As explained in the reprint of our Physical Review Letters article (Appendix A), our semiclassical perturbation approach is equally applicable to treating the interaction of an electron with a neutral dipole. Under the sponsorship of other agencies, and with SRI internal research funds, we have devoted considerable effort to computing the elastic and rotationally inelastic cross sections for electron impact on highly polar neutral molecules such as CsF and KI. Our interest in these two systems arose because these cross sections have been measured experimentally by Stern and his students[8,9] at Columbia University and, furthermore, they have been[10] and currently are the subject of study at other laboratories using the close-coupling quantum mechanical approach.

We have now used the semiclassical S-matrix to compute the total scattering cross section (elastic and rotationally inelastic) for a test case in the scattering of an electron by CsF at 1 eV with the polar molecule initially in the rotational state with $j = 41$. We have been able to compare the results with calculations by Norcross and Collins

at JILA (Boulder, Colorado) who have done it with a Born approximation and, for smaller quantum numbers, the close-coupling calculations. Our results deviate significantly from the close-coupling results only at very small values of orbital angular momentum quantum numbers, namely for $\ell \leq 2$. In this region the Born approximation is totally inadequate and it does not converge to the semiclassical values until about $\ell = 7$.

The ability of the perturbation semiclassical approach to successfully treat the electron-polar molecule interaction problem at all but the smallest quantum numbers demonstrates the great flexibility of our method. It is particularly noteworthy that our method, in contrast to either the exact quantum mechanical or the fully classical approach, enables us to understand both qualitatively and quantitatively the contributions corresponding to essentially classical scattering, to quantum interference effects, and to tunneling into a classically forbidden region. As for the failure of the semiclassical method at the few lowest lying orbital angular momentum quantum numbers, we believe that there is considerable scope for refining our approach so as to reduce the discrepancy between the close coupling and semiclassical results in this quantum number regime. This could be achieved by (a) removing the perturbation approximation and instead using the numerical solution of the exact classical equations of motion of the system for computing the S-matrix elements and (b) using a more realistic short range potential by supplementing the charge-dipole interaction term with higher order multipole and polarizability terms.

Returning to the ion-ion mutual neutralization problem, we feel that, due to the long range nature of the coulombic forces, the total orbital capture cross sections are likely to be dominated by contributions from trajectories characterized by relatively large distances of closest approach. The results of our preliminary calculations for the

capture of O^- by NO^+ lend strong support to this view. Hence we expect the perturbation semiclassical approach as it stands to be adequate for the calculation of reliable ion-ion neutralization cross sections. The considerations relating to electron-polar molecules discussed in the previous paragraph are, however, relevant to the question of calculation of electron-ion recombination cross sections and we anticipate that our semiclassical method will be extremely useful for this purpose.

DISCUSSION OF THE EFFECTS OF CLUSTERING ON ION STABILITY AND NEUTRALIZATION RATES

We consider our discovery of a closed-form perturbation solution for the general scattering problem for the ion-dipole ion system, including capture collisions, to be of the greatest importance. Not only does it allow rapid and economical estimation of capture cross section and rates, but even more important, it makes possible a methodical investigation of the effect of changing conditions and parameters. As our experience with the properties of this solved problem grows we expect our understanding to become much more complete and secure, and we will then be able to extend it to the related but somewhat more complex problems that arise in considering the neutralization of clustered ions.

The commonest clustering species associated with most ions in the lower ionosphere, both positive and negative, is water. The most important clustered ions, therefore, have highly polar components (water molecules) very much subject to the effects of transient electrostatic forces caused by a passing ion of opposite sign. In most cases the clustered ions are expected to be very soft, with bending modes of low frequency exceptionally easily excited, since the ion-dipole attraction that creates the clustering is generally less strongly directionally dependent than most chemical bonds. Furthermore, a comparatively simple electrostatic model for the structure allows reasonable, if rough, estimation of the restoring forces and the characteristic bending frequencies. Information of this type is needed to develop a more quantitative approach to the neutralization rates of these clustered species.

As part of our program we intend to extend our approach from rotational excitation of diatomic molecules to the excitation of bending modes, i.e., internal rotations in a simple hydrated ion (for instance, an ionic core such as an alkali ion with a single attached water molecule).

Generally, hydration will have three effects on an isolated molecular ion: it will increase the stability of the ion (whether it is positive or negative); it will increase the number of degrees of freedom of the molecule; and especially it will produce low frequency internal modes (soft bending vibrations). Increasing the stability of the negative ion contracts the exponential tail of the electron cloud and causes more rapid fall-off with distance of the overlap matrix $H_{12}(R)$, leading generally to a lower neutralization cross section. At the same time, increased stability of the ions relative to the neutrals causes all the neutral molecular potential curves of the combined molecule to move upward relative to the coulombic ion-ion potentials, and causes each crossing point to move outward to larger R. In general, therefore, hydration tends to reduce the cross section for neutralization by electron capture (as described by the curve-crossing model). On the other hand, by increasing the number of internal degrees of freedom, and especially of the soft bending modes that can easily be excited by the tidal forces associated with the close passage of a second ion of opposite charge, increasing hydration is associated with an increasing cross section for neutralization by tidal capture. This is a totally different mechanism from electron transfer (although temporary capture can sometimes also allow multiple passages past the crucial curve-crossings, thus enhancing the opportunities for electron transfer). Thus, in general, we can envisage the possibility that hydration may have two competing effects on ionic neutralization rates: it decreases

the electron-transfer rate, and it ultimately compensates by increasing the tidal recombination rate. In some cases, and perhaps in many, the combined effect may lead to a minimum in the recombination rate as a function of n, the degree of hydration of one of the ions, at some small value, perhaps n = 1 or 2.

These effects can be enhanced further by the occurrence of special structural configurations. We have, therefore, been led to consider the structures associated with hydration in positive and negative ions.

In the case of water attached to a positive ion, the principal binding can be considered to arise from simple ion-dipole binding. In the case of hydrated negative ions, on the other hand, it seems likely that the attachment of a water molecule will be centered at one of the H atoms, and that a form of hydrogen bond is likely to result. Ordinary hydrogen bonds tend to be comparatively straight, with the H atom roughly on the line of centers between its two neighbors, but usually asymmetrically placed much closer to the atom with which it has its primary chemical bonding. Under very exceptional conditions, however, symmetrical hydrogen bonds have recently been observed. Pauling[11] estimates the typical restoring constant for the bending of a hydrogen bond in water to be 0.003 kcal/mole-deg^2. Whether this is a typical figure that can be used for estimating bending force constants in hydrated negative ions is uncertain, but it at least provides some guidance.

In some cases, exceptional structures may exist that will provide special stability to certain ions, and cause various parameters, including bending force constants, to deviate from the general pattern. As an example, let us consider the special case of the ion $NO_2^-.H_2O$. This is probably the principal ion of mass 64 observed in a decaying plasma in air by Dr. Merle Hirsch (reported at the 28th Gaseous Electronics Conference on October 21-24, 1975). This ion apparently

recombines exceedingly slowly, with a rate coefficient of about 10^{-8} cm^2/sec, and appears to have unusually high mobility for a negative ion. It would be of considerable interest to make further measurements on this ion and even to determine its structure. Several possible structures can be considered.

Structure A, illustrated in Fig. 2, appears to be a plausible chemically bonded form for what may be the lowest stable state of the ion $H_2NO_3^-$. In that case, the three oxygen atoms may be bonded to nitrogen roughly as in NH_3 (i.e., in a pyramidal structure). This structure is not a simple hydrate, but requires considerable rearrangement, and if it is produced at all, it is, no doubt, the result of a more complicated series of steps than simple hydration. It might, therefore, be more common under high-pressure conditions than at low.

Structure B represents a typical hydrate of NO_2^-, assuming a standard, almost linear, hydrogen bond. Such a structure is rather open and loose and subject to fairly free rotation of the components about the H-bond, but electrostatic forces arising from the contributing structure B' may make the coplanar structure somewhat more stable.

One can also speculate on the possibility of a more symmetric coplanar structure as illustrated in C, which might also have significant contributions of the companion structure D. These structures have the possibility of additional stabilization through delocalization of the electron and formation of a second hydrogen bond, but this is achieved at the expense of bending the hydrogen bond and possibly by forcing the hydrogen to a more symmetric position. If the structure C (and D) exists, it is sure to be coplanar and rather stiff in its bending modes, and this will have consequences for both the energetics and the entropy of the molecule. A theoretical examination of these possible structures as well as further experimental studies of the properties of this hydrated ion would be well warranted. If

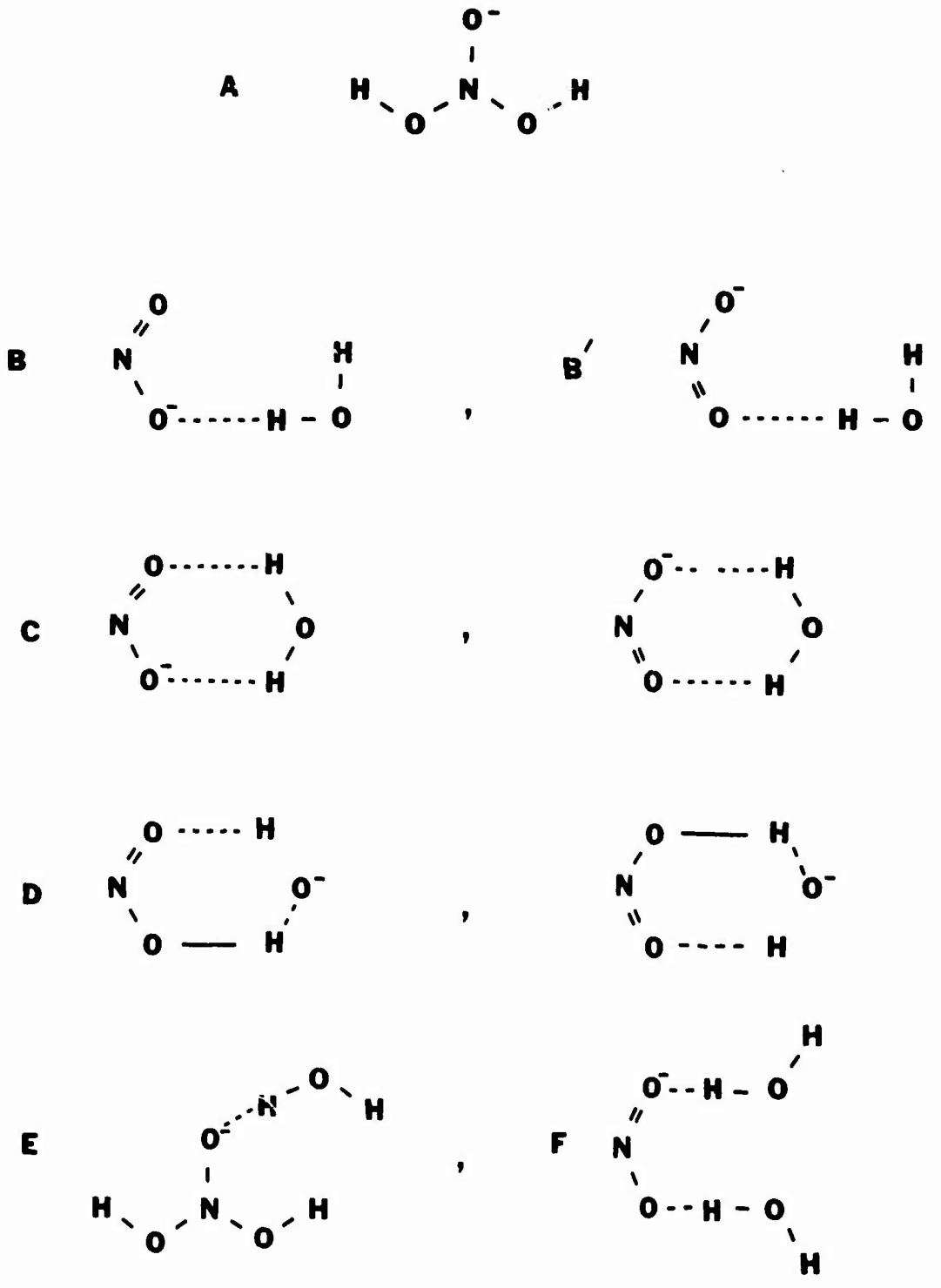

FIGURE 2 STRUCTURES: $NO_2^- . H_2O = H_2NO_3^-$ (MASS=64)

it has a compact structure like either A or C, its exceptionally low recombination rate might be understood.

Once the ion is doubly hydrated, a much looser structure generally results, with very significant softening of the bending modes as well as other consequences such as increased size and lower mobility. Among the possibilities are such structures as E and F, of which E is obviously derived from A and F from B or C.

If the ring structures we have discussed here are valid in $NO_2^-.H_2O$, they may also apply to other negative ions such as NO_3^- and CO_3^- when they are singly hydrated. In that case a number of important singly hydrated ions may be quite different in their properties from the higher hydrates. These effects would appear both in the thermodynamics of the ions and their spectroscopy, and also in other properties such as neutralization rates, photodissoci tion and photodetachment, and possibly in such collision properties as mobility.

These arguments suggest that singly hydrated ions will often have rather special properties. Their electrons will be more strongly bound than those of the parent unhydrated ions, which will tend to result in lower neutralization rates by the electron transfer (curve-crossing) mechanism. On the other hand, having stiff and compact structures, they will also have rather low cross sections and rates for tidal capture into an elliptical orbit by ions of opposite charge, the process that we expect to be rate-determining for recombination of large cluster-ions at low pressure.

REFERENCES

1. F. T. Smith, D. L. Huestis, D. Mukherjee, and W. H. Miller, Phys. Rev. Letters 35, 1073 (1975).

2. R. A. Bennett, J. T. Moseley, and J. R. Peterson, J. Chem. Phys. 62, 2223 (1975).

3. J. T. Moseley, R. E. Olson, and J. R. Peterson in "Case Studies in Atomic Physics," edited by M. R. C. McDowell and E. W. McDaniel (North Holland Publishing Company, Amsterdam), Vol. 5, pp. 1-45, 1975.

4. R. A. Bennett, D. L. Huestis, J. R. Moseley, D. Mukherjee, R. E. Olson, S. W. Benson, J. R. Peterson, and F. T. Smith, "Investigation of Ion-Ion Recombination Cross Sections," Report No. AFCRL-TR-74-0417, Contract F19628-72-C-0121, 27 November 1974.

5. R. J. Cross, J. Chem. Phys., 46, 609 (1967).

6. W. H. Miller, J. Chem. Phys. 53, 1949 (1970).

7. W. H. Miller, J. Chem. Phys. 54, 5386 (1971).

8. R. C. Slater, et al., J. Chem Phys. 60, 4697 (1974).

9. R. C. Slater, et al., J. Chem Phys. 61, 2290 (1974).

10. A. C. Allison, J. Phys. B. 8, 325 (1975).

11. L. Pauling, The Nature of the Chemical Bond (Cornell University Press, Ithaca, New York, 1960, 3rd ed.) p. 453.

APPENDIX A

VOLUME 35, NUMBER 16 PHYSICAL REVIEW LETTERS 20 OCTOBER 1975

Semiclassical Perturbation Scattering by a Rigid Dipole*

F. T. Smith, D. L. Huestis, and D. Mukherjee
Stanford Research Institute, Menlo Park, California 94025

and

W. H. Miller
Department of Chemistry, University of California, Berkeley, California 94720

(Received 31 July 1975)

A uniform semiclassical S matrix has been developed for collisions of charged particles with rotating rigid dipoles, with use of first-order perturbation theory. The resulting expression is analytical, depending on tabulated functions, and trivial to calculate; it allows evaluations of quantum transitions in classically forbidden regions, and of quantum interference effects.

In the course of studies of the scattering of electrons and ions by simple polar molecular targets, we have discovered a versatile analytical form for the S matrix in the limit of semiclassical perturbation theory when the anisotropic part of the interaction is dominated by a dipole term.

Cross[1] developed a classical perturbation theory of ion-molecule, including ion-dipole, scattering in a formulation emphasizing angular coordinates and spherical trigonometry. We find it advantageous to make maximum use of angular momentum conservation, formulating the problem in the classical version[2,3] of a (J, M, j, l) angular momentum coupling, where j is the angular momentum of the target molecule and l is the collisional angular momentum, while J and M refer to the total angular momentum and its projection. [Where the distinction is important, j, l, and J will be used for quantum numbers, and the corresponding classical angular momenta are given by expressions like $j^{cl} \cong (j+\frac{1}{2})\hbar$.] We have used the semiclassical S-matrix formulation of Miller,[3] combined with first-order perturbation dynamics. By applying a canonical Hamiltonian transformation, we find the phase of the S matrix to have a contribution not identified by Cross.

The uniform semiclassical form for the S matrix provides an appropriate estimate of quantum effects in the nonclassical tunneling region and at the classical turning points, as well as interference effects in the classically allowed region. In addition, by use of the semiclassical S matrix in (J, M, j, l) coupling followed by quantal recoupling using 6-j symbols and construction of the scattering amplitude using the Wigner rotation matrices, we can obtain the quantal diffraction effects in small-angle scattering.

We consider a problem with a zero-order potential interaction in which $\vec{j}$ and $\vec{l}$ are separately conserved:

$$V_0 = V_0(R). \tag{1}$$

R is the radial coordinate associated with the collision. In the plane determined by $\vec{l}$, the unperturbed collisional motion follows a classical trajectory given by $R(t)$ and $\Phi(t)$, and in the plane determined by $\vec{j}$ the rotor's unperturbed motion is given by $\Theta(t)$. The angle κ between the two planes is fixed by the magnitudes j, l, and J:

$$N = \cos\kappa = \frac{\vec{j}\cdot\vec{l}}{|\vec{j}||\vec{l}|} = \frac{(j+\frac{1}{2})^2 + (l+\frac{1}{2})^2 - (J+\frac{1}{2})^2}{2(j+\frac{1}{2})(l+\frac{1}{2})}. \tag{2}$$

The line of intersection of the two planes—or the plane perpendicular to it—defines a reference direction for the measurement of Φ and Θ, each in its own plane. It is convenient to take $t=0$ at a central point in the trajectory, and assume the unperturbed $R(t)$ to be an even function of t. We can then write $\Theta(t) = \Theta_0 + \bar{\Theta}(t)$ and $\Phi(t) = \Phi_0 + \bar{\Phi}(t)$, where $\bar{\Theta}(t)$ and $\bar{\Phi}(t)$ are odd functions of t.

The anisotropic interaction will be treated as a perturbation (to which an isotropic part can be added as well). Particular simplifications occur for a dipole interaction, and our attention will be limited to that case; extensions to higher multipoles and nonrigid targets are possible, but they will probably entail greater reliance on numerical methods. We shall assume the general form of the interaction to be

$$V_1(R,\gamma) = U(R)\cos\gamma, \tag{3}$$

where

$$\begin{aligned}\cos\gamma &= -\cos\Phi\cos\Theta + N\sin\Phi\sin\Theta \\ &= -\tfrac{1}{2}(1+N)\cos\psi_+(t) \\ &\quad -\tfrac{1}{2}(1-N)\cos\psi_-(t),\end{aligned} \tag{4}$$

with

$$\psi_\pm(t)=\Theta(t)\pm\Phi(t)=\psi_\pm^0+\Psi_\pm(t), \tag{5}$$

and

$$\psi_\pm^0=\Theta_0\pm\Phi_0, \quad \Psi_\pm(t)=\bar{\Theta}(t)\pm\bar{\Phi}(t). \tag{6}$$

The dynamic effects of the perturbation can now be evaluated. The associated action integral is a function of Θ_0 and Φ_0,

$$A=A(\Theta_0,\Phi_0)=\int_{-\infty}^{\infty}V_1(R(t),\cos\gamma(t))\,dt. \tag{7}$$

This is conveniently simplified through use of the angular variables $\psi_\pm^0$ and $\Psi_\pm(t)$:

$$\begin{aligned}A&=\bar{A}(\psi_+^0,\Psi_-^0)\\&=-\tfrac{1}{2}(1+N)B_+\cos\psi_+^0\\&\quad-\tfrac{1}{2}(1-N)B_-\cos\psi_-^0,\end{aligned} \tag{8}$$

where

$$B_\pm=\int_{-\infty}^{\infty}U(R(t))\cos\Psi_\pm(t)\,dt. \tag{9}$$

Solving the Hamiltonian equations of motion for the changes in l and j to first order, one can easily show that

$$\hbar\Delta l=-\frac{\partial A(\Theta_0,\Phi_0)}{\partial\Phi_0}, \quad \hbar\Delta j=-\frac{\partial A(\Theta_0,\Phi_0)}{\partial\Theta_0}. \tag{10}$$

If we define

$$\Delta k_\pm=\tfrac{1}{2}(\Delta j\pm\Delta l), \tag{11}$$

and

$$Z_\pm=(2\hbar)^{-1}(1\pm N)B_\pm, \tag{12}$$

we have the simple result

$$\Delta k_\pm=-\hbar^{-1}\partial\bar{A}/\partial\psi_\pm^0=-Z_\pm\sin\psi_\pm^0. \tag{13}$$

The range of classically accessible values of Δk_+ and Δk_- is determined by $Z_\pm$, which depends on the unperturbed values of l and j, on J, and on the collisional energy E. In addition, each value of Δk_+ or Δk_- is associated with a pair of permissible values for the associated angle ψ_+^0 or ψ_-^0, so that each set of values $(\Delta k_+,\Delta k_-)$ can be reached by four different classical trajectories. These will lead to an interference pattern in the S matrix.

The classical phase is expressed by

$$\begin{aligned}\varphi&=-\int dt\,[R'(t)\dot{p}'(t)+\Phi'(t)\dot{l}'^{\rm cl}(t)+\Theta'(t)\dot{j}'^{\rm cl}(t)]\\&=\int dt\left[R'(t)\frac{\partial V_1}{\partial R'}+\Phi'(t)\frac{\partial V_1}{\partial\Phi'}+\Theta'(t)\frac{\partial V_1}{\partial\Theta'}\right],\end{aligned} \tag{14}$$

where R', p', etc., are "new" variables (related to the original variables R, p, etc., through a canonical transformation) chosen in such a way that the coordinates R, Θ', and Φ' appear explicitly only in the perturbation potential term (V_1) in the transformed Hamiltonian. With the help of the appropriate canonical transformation, it can be shown that

$$\begin{aligned}\varphi&=-\Theta_0\hbar\Delta j-\Phi_0\hbar\Delta l-A(\Theta_0,\Phi_0)\\&=-\psi_+^0\hbar\Delta k_+-\psi_-^0\hbar\Delta k_--\bar{A}(\psi_+^0,\psi_-^0).\end{aligned} \tag{15}$$

Making the appropriate substitutions, we can write this in the form

$$\varphi/\hbar=\eta_++\eta_-, \tag{16}$$

where

$$\begin{aligned}\eta_\pm&=-\psi_\pm^0\Delta k_\pm+Z_\pm\cos\psi_\pm^0\\&=(Z_\pm^2-\Delta k_\pm^2)^{1/2}+\Delta k_\pm\sin^{-1}(\Delta k_\pm/Z_\pm).\end{aligned} \tag{17}$$

To construct the S matrix, we need the Jacobian D as well as the phase φ:

$$\begin{aligned}D&=\frac{\partial(j,l)}{\partial(\Theta_0,\Phi_0)}=\frac{\partial(\Delta j,\Delta l)}{\partial(\Theta_0,\Phi_0)}\\&=4\frac{\partial\Delta k_+}{\partial\psi_+^0}\frac{\partial\Delta k_-}{\partial\psi_-^0}=C_+C_-,\end{aligned} \tag{18}$$

if we take

$$\begin{aligned}C_\pm&=-2\frac{\partial\Delta k_\pm}{\partial\psi_\pm^0}=2Z_\pm\cos\psi_\pm^0\\&=2(Z_\pm^2-\Delta k_\pm^2)^{1/2}.\end{aligned} \tag{19}$$

The symmetry of the solutions is such that nothing is changed if we replace (Θ_0,Φ_0) by $(\Theta_0+\pi,\Phi_0+\pi)$, which leads to a selection rule of $\Delta k_\pm$ = integer.

The S matrix is the sum of four terms, corresponding to the four pairs of roots (ψ_+^0,ψ_-^0) allowed by Eq. (13), each being of the form

$$[(2\pi i)^2D]^{-1/2}\exp(i\varphi/\hbar). \tag{20}$$

Exercising appropriate care to identify the phases, and making use of the form of D and φ, we find that we can combine terms so that S can be factored into two independent portions,

$$S=S_+S_-, \tag{21}$$

where

$$S_\pm=(4/\pi C_\pm)^{1/2}\sin(\tfrac{1}{4}\pi+\beta_\pm) \tag{22}$$

with

$$\beta_\pm=\tfrac{1}{2}C_\pm+\cos^{-1}(-\Delta k_\pm/Z_\pm). \tag{23}$$

This form is appropriate well into the classical

region of motion, $\Delta k_\pm^2 \ll Z_\pm^2$, or $C_\pm^2 \gg 0$. Quantum effects become important near $C_\pm = 0$, and there we can make use of a uniform approximation in the Bessel function form,[4,5] which reduces to (22) in the limit of large $C_\pm$:

$$S_\pm = J_{\Delta k_\pm}(Z_\pm). \tag{24}$$

When $C_\pm$ becomes imaginary, (24) goes over into an exponential tunneling form valid for $\Delta k_\pm^2 \gg Z_\pm^2$, or $C_\pm^2 \ll 0$:

$$S_\pm \sim (\pi|C_\pm|)^{-1/2}\exp(-|\beta_\pm|). \tag{25}$$

The form (24), however, is valid everywhere, and is essential near the edge of the classical region, where $C_\pm^2 \sim 0$, i.e., at the classical turning points.

The S matrix is desired in terms of the initial and final angular momenta, which are connected with j, l, Δj, and Δl by

$$\begin{aligned} l_1 &= l - \Delta l/2, \quad l_2 = l + \Delta l/2, \\ j_1 &= j - \Delta j/2, \quad j_2 = j + \Delta j/2. \end{aligned} \tag{26}$$

Also the initial and final collisional energies are connected with the average value E by

$$\begin{aligned} E + (j+\tfrac{1}{2})^2\hbar^2/2I &= E_1 + (j_1+\tfrac{1}{2})^2\hbar^2/2I \\ &= E_2 + (j_2+\tfrac{1}{2})^2\hbar^2/2I. \end{aligned} \tag{27}$$

With use of these relations [(26) and (27)] and the properties of the Bessel functions, it is easy to show that this S matrix is correctly symmetric and approximately unitary—approaching unitarity correctly as l and j grow large. It is not difficult to renormalize it for small j and l to make it correctly unitary.

We have evaluated the integrals $B_\pm$ [Eq. (9)] for two specific cases, in both of which the perturbation is an ion- or electron-dipole interaction,

$$V_1 = (\mu e/R^2)\cos\gamma. \tag{28}$$

When the target is a neutral dipole, case (a), the unperturbed potential vanishes, $V_0 = 0$. The result can be expressed in terms of a parameter measuring the ratio of angular velocities of the rotor and the collisional motion at $t = 0$,

$$\omega_a = (j+\tfrac{1}{2})(l+\tfrac{1}{2})\hbar^2/2IE, \tag{29}$$

where I is the moment of inertia of the dipole, a factor

$$m\mu e^2/\hbar^2(l+\tfrac{1}{2}), \tag{30}$$

where m is the reduced mass in the collision, and the integrals

$$I_{\pm,a} = \omega_a[K_1(\omega_a) \mp K_0(\omega_a)]. \tag{31}$$

The same integrals appear in the problem as formulated by Cross,[1] and also in Percival's theory of excitation of hydrogenic atoms by charged particles.[6] Then the quantity $Z_\pm$ becomes

$$Z_\pm = (m\mu e/\hbar^2)(l+\tfrac{1}{2})^{-1}(1 \pm N)I_{\pm,a}(\omega_a). \tag{32}$$

We are using this solution in a study of scattering and rotational excitation in collisions of electrons or ions with polar molecules.

When the dipolar target has a net charge, and the bombarding species is an ion, V_0 is the Coulomb potential, $V_0 = \pm e^2/R$. We have found an interesting solution for a special case, where the unperturbed collisional energy E is 0 and the trajectory is parabolic. In that case, (b), we have

$$\omega_b = (j+\tfrac{1}{2})(l+\tfrac{1}{2})^3\hbar^4/me^4I, \tag{33}$$

and the integrals $I_{\pm,b}$ lead to Airy functions,

$$\begin{aligned} I_{\pm,b} &= 2\pi[+x\,\mathrm{Ai}(x) - x^{1/2}\mathrm{Ai}'(x)], \\ x &= (\tfrac{1}{2}\omega_b)^{2/3}. \end{aligned} \tag{34}$$

This solution is of interest in connection with capture or detachment between free (hyperbolic) trajectories with eccentricity slightly greater than 1, and large elliptic orbits with eccentricity slightly less than 1.

The separation of the equations connecting the phase angles $\psi_\pm^0$ with the momenta $\Delta k_\pm$ in the simple form of Eq. (13) appears to be peculiar to the dipole angular dependence of V_1. It is independent of the R dependence of V_0 and V_1, and so the factorization of the S matrix and the general form (24) of its factors persists, only the integrals $B_\pm$ or $I_\pm$ changing with the functional form of the R dependence. These integrals can be obtained by numerical quadrature when an analytical form is not available.

When the angular dependence of V_1 is not that of a simple dipole, $P_1(\cos\gamma)$, the elimination of the phase angles and the expression of S as a function of the angular momenta and their perturbations is not so simple as in the dipole case, and may have to be carried out by numerical interpolation. In that case, the S matrix will probably not factorize.

*Work supported by the U. S. Air Force Cambridge Research Laboratories, the National Science Foundation, the U. S. Air Force office of Scientific Research,

and Stanford Research Institute internal research funds.

[1]R. J. Cross, J. Chem. Phys. 46, 609 (1967).

[2]E. A. Whittaker, *Analytical Dynamics* (Cambridge Univ. Press, Cambridge, England, 1931), pp. 348–351.

[3]W. H. Miller, J. Chem. Phys. 54, 5386 (1971).

[4]J. R. Stine and R. A. Marcus, J. Chem. Phys. 59, 5145 (1973).

[5]W. H. Miller, in "Advances in Chemical Physics," edited by K. P. Lawley (Wiley, New York, to be published), Vol. 30.

[6]I. C. Percival, J, Phys. B: At. Mol. Phys. 6, 2236 (1973).

APPENDIX B

Electron loss cross sections for O^-, O_2^-, NO_2^-, and NO_3^- in several gases*

R. A. Bennett†, J. T. Moseley, and J. R. Peterson

Stanford Research Institute, Menlo Park, California 94025
(Received 18 November 1974)

The cross sections for electron loss for O^-, O_3^-, NO_2^-, and NO_3^- on He, N_2, and Ar, for O^- on O_2, and NO_3^- on NO_2 have been measured using a beam attenuation technique. The measured cross sections are the sum of collisional detachment and electron transfer cross sections. Except for $O^- + O_2$, the cross sections are nearly constant for ion energies in the range 1 to 4 keV and generally increase with target mass.

INTRODUCTION

We report the measurement of electron loss cross sections for O^-, O_2^-, NO_2^-, and NO_3^- in several gases. The work originated in an attempt to determine any excited state fractions of negative ion beams used in this laboratory for ion–ion recombination rate measurements.[1] A beam attenuation technique similar to that of Turner *et al.*[2,3] was used. No evidence for suspected excited state ions was found, but the experimental setup made it possible to determine electron loss cross sections. The total loss cross section which is here associated primarily with collisional detachment, may be determined by measuring the current I remaining when an ion beam of initial current I_0 traverses a distance l through a chamber containing a gas with number density n. If the beam contains two components (such as a ground state and an excited state) in fractional amounts f_1 and $f_2 = 1 - f_1$, with different loss cross sections Q_1 and Q_2, respectively, the current collected will be

$$I = I_0[f_1 e^{-nlQ_1} + (1 - f_1)e^{-nlQ_2}]. \quad (1)$$

A plot of log (I/I_0) versus pressure will thus show a curve with different low-pressure and high-pressure asymptotic slopes. The two slopes determine the two characteristic cross sections Q_1 and Q_2, and the zero pressure intercepts yield f_1 and f_2. For every case reported here, the attentuation curve of log I/I_0 versus pressure appears to be a single straight line, indicating a single state for the ions in the beam, or at least that the products fQ for all components were the same to within about 5%. The possiblility of loss mechanisms other than collisional detachment will be discussed below

APPARATUS

The apparatus is a merged beams system[1] which was modified to make attenuation measurements as shown in Fig. 1. Negative ions extracted from a duoplasmatron ion source were accelerated to the beam energy of 1 to 4 keV. After mass selection by a crossed fields velocity filter, the ions were focused and deflected through a 1 cm aperature into an attenuation chamber. The focused beams were usually less than 0.6 cm in diameter, so that losses to the aperture boundaries were negligible. After traveling a length $l = 34.3$ cm, the beam was collected in a shielded Faraday cup and monitored by an electrometer. The secondary electron suppression grid in front of the Faraday cup was maintained at -30 V, thus also preventing collection of slow electrons that were collisionally detached in the target gas along the beam path. Tests using a two-part concentric Faraday cup established that scattering losses of the beam were insignificant. Differential pumping limited the measured attenuation to the last chamber.

The attenuation chamber pressure was measured using a Pirani gauge and a Varian nude ion gauge, each of which was calibrated against an MKS Baratron capacitance manometer down to 10^{-4} Torr. Both gauges were observed to be quite linear with pressure above 10^{-4} Torr, and were assumed to be linear down to 10^{-5} Torr. The ion gauge was used for the pressure measurements on the rare gases and on N_2, and the Pirani gauge was used for O_2 and NO_2, because for these gases stability problems were encountered when using the ion gauge. However, some attenuation measurements were made on each gas using both gauges.

As a test of the experimental technique, the attenuation by argon of 3 keV NO^+ ions from a duoplasmatron source was studied. The attenuation curve showed a two-slope behavior similar to that seen by Mathis *et al.*[3] Most of the NO^+ beam had an attenuation cross section of 16×10^{-16} cm^2. A small fraction of the NO^+ beam, about 15%, had a much larger cross section. The exact fraction depended on the ion source parameters, including the gas mixture and the pressure.

With the use of various mixtures of O_2, NO, and NO_2 in the negative ion source, beams of 10^{-6} A of O^-, 10^{-6} A of O_2^-, 10^{-9} A of NO_2^-, and 10^{-9} A of NO_3^- could be obtained. The ion source pressure was in the range of 10 to 100 mTorr. Only long-lived ion states contributed to the attenuation measurements, because the minimum flight time from ion source to attenuation chamber is 7 μsec with 4 keV O^- ions.

RESULTS

The attenuation of a 3.75 keV beam of O_2^- ions by nitrogen is shown in Fig. 2. The logarithm of the collected current was plotted versus the nitrogen pressure indicated by an ion gauge. The residuals of a straight line, least squares fitted to the data, showed no systematic variation. For the same beam energy and target, the linearity and slope of the attenuation curve were very reproducible. The slope of the attenuation curve as plotted in Fig. 2 yielded a cross section of 12.8 ± 1.2

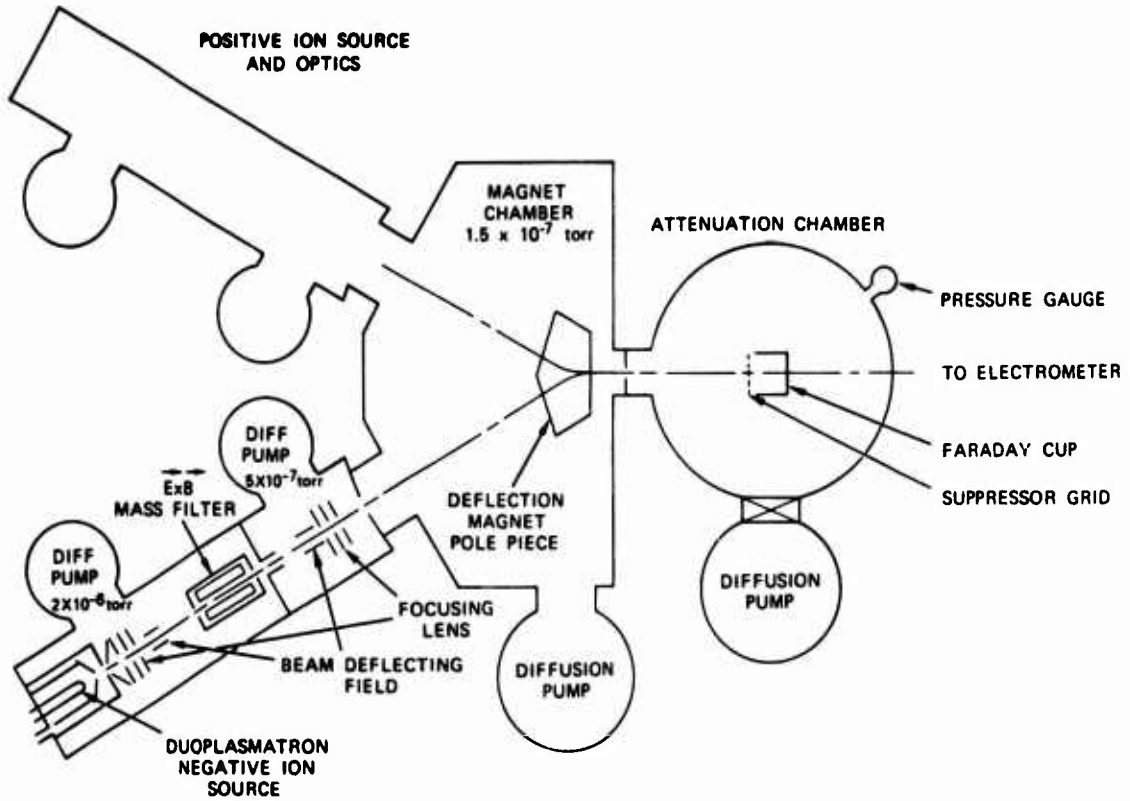

FIG. 1. Experimental apparatus.

$\times 10^{-16}$ cm^2 for the attenuation of 3.75 keV O_2^- by nitrogen, using Eq. (1) with $f_1 = 1$ and after corrections to the gauge pressure readings. The uncertainty in the absolute magnitude of the cross section so determined arose from the uncertainties in current and pressure measurement. The uncertainty in the current measurement was taken to be twice the rated electrometer accuracy, or 4%. The uncertainty in the pressure measurement was conservatively placed at ±15% in He and O_2, ±13% in Ar, and ±5% in N_2 and NO_2.

The attenuation cross sections for O^-, O_2^-, NO_2^-, and NO_3^- in various gases as functions of laboratory ion energy are shown in Figs. 3–6. The cross sections, at a representative 3 keV ion energy, are tabulated in Table I. In He, O_2, and NO_2, which may form negative ions, the electron loss cross section is the sum of cross sections for charge exchange and collisional detachment.

In addition to single electron loss collisions, with whose cross sections σ_{-10} we are primarily concerned here, we must consider two-electron loss collisions which form positive ions in the beam and subtract from the negative ion current. Thus, as Risley and Geballe[4] have pointed out, these negative ion attenuation measure-

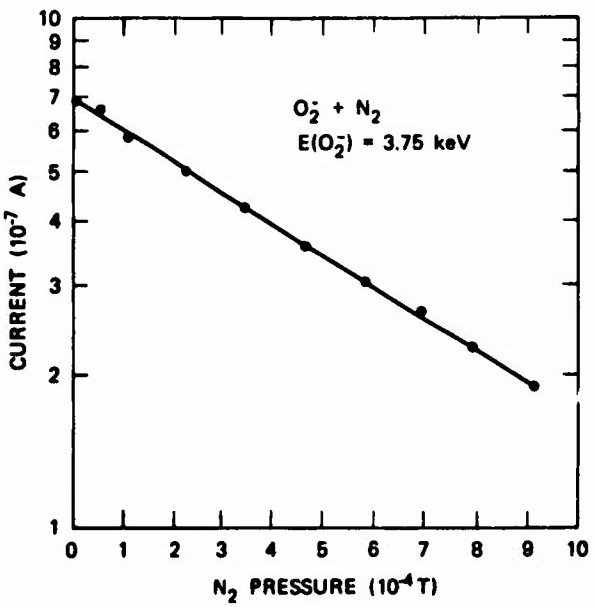

FIG. 2. Attenuation of O_2^- by N_2.

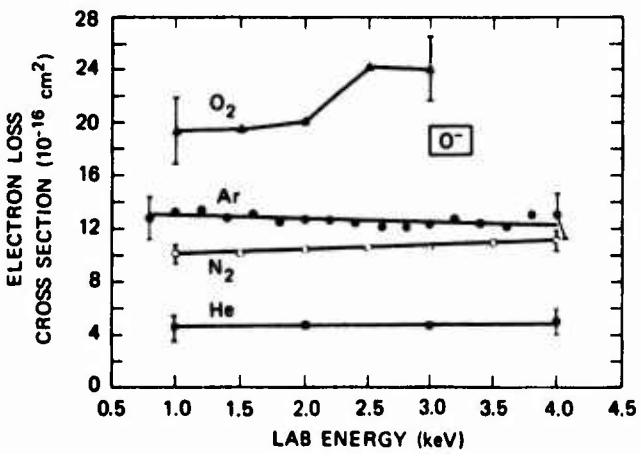

FIG. 3. Electron loss cross sections for O^-.

TABLE I. Electron loss cross sections for O^-, O_2^-, NO_2^-, and NO_3^- at 3 keV.

	$\sigma(10^{-16}\text{cm}^2)$			
	O^-	O_2^-	NO_2^-	NO_3^-
He	4.6	4.4	5.0	7.0
N_2	10.7	13.1	16.0	15.5
O_2	24	•••	•••	•••
Ar	12.5	21.8	16.0	18.3
NO_2	•••	•••	•••	39.5

ments in principle measure single collision cross sections containing $\sigma_{-10}+2\sigma_{-11}$, and at high energies one should consider even higher ionization processes. In the present case, however, σ_{-11} is probably at least 20 times smaller than σ_{-10}, judging from the low energy trends in the cross sections obtained by Matić and Čobić.[5] We therefore consider these measurements to represent primarily single electron loss cross sections σ_{-10}. In most cases the loss mechanism is collisional detachment. However, in the cases of O_2 and NO_2 targets which have positive electron affinities, charge transfer may also be an important process. Unfortunately only one measurement was made in each of these gases. Charge transfer to He, which has an excited negative ion state, is about 19 eV endothermic and is almost certainly negligible. Similarly, excitation of the 2 eV excited virtual state in N_2^- is probably unimportant as a loss channel. Some of these effects will be considered below.

DISCUSSION

In Fig. 7 the attenuation cross sections for O^- in He and Ar are plotted against O^- velocity and can be compared with other results. The He results are in quite good agreement with Hasted's results[6] which also agree with the low energy data given by Wynn, Martin, and Bailey (WMB).[7] No uncertainty estimates are given by Hasted, and it is not apparent that the 15% difference in results is significant. The relative consistency among our data points indicates that there is little, if any, energy dependence in the cross section at these energies.

The O^- + Ar results of Hasted are about 30% lower than ours and again match the WMB data at low energy. The results of Roche and Goodyear[8] are slightly below those of

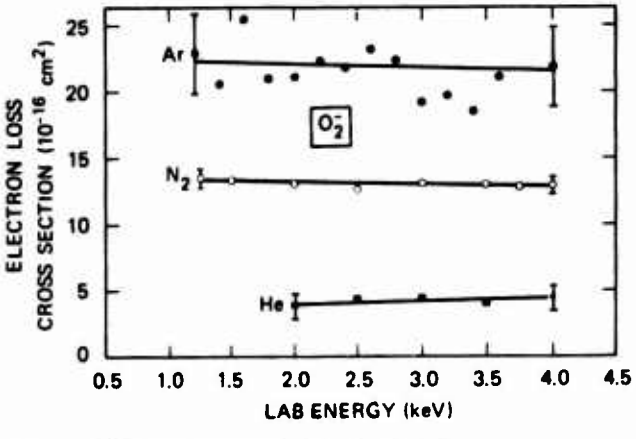

FIG. 4. Electron loss cross sections for O_2^-.

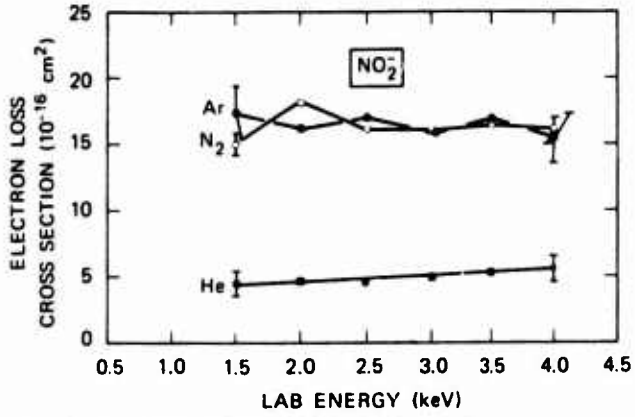

FIG. 5. Electron loss cross sections for NO_2^-.

WMB. Between the speeds of 10 and 22×10^6 cm/sec, the Hasted results for both He and Ar show a slight increase, while our cross sections are essentially constant. The results of Matić and Čobić[5] on O^- + Ar begin at 8 keV, and therefore it is not possible to compare them directly with our results or those of Hasted. However, if the results at 4 and 8 keV are both correct in absolute magnitude, the cross section must exhibit an unexpectedly strong energy dependence in the energy region between the measurements.

A comparison with other results for O^- in N_2 and O_2 is made in Fig. 8. The results of Hasted and Smith[9] for O^-+N_2 are about 20% below ours and show a slight decrease with speed while our results show a slight increase. Apparently the O^-+N_2 cross section is about constant in this energy range. The results of Matić and Čobić for O^-+N_2 extend down to 5 keV and again are substantially below our results at 4 keV.

The O^-+O_2 data are in reasonably good agreement with Hasted and Smith in both magnitude and energy dependence. The results of Bailey and Mahadevan[10] and Ranjan and Goodyear[11] are somewhat lower. The cross section is larger than would be expected from the relative size of O_2 compared to N_2 and Ar. The energy dependence in the 1–4 keV range is in distinct contrast to that for He, Ar, and N_2. This can be explained by the open charge transfer channel, $O^-+O_2 \rightarrow O+O_2^-$, which supplements collisional detachment as a loss mechanism. The

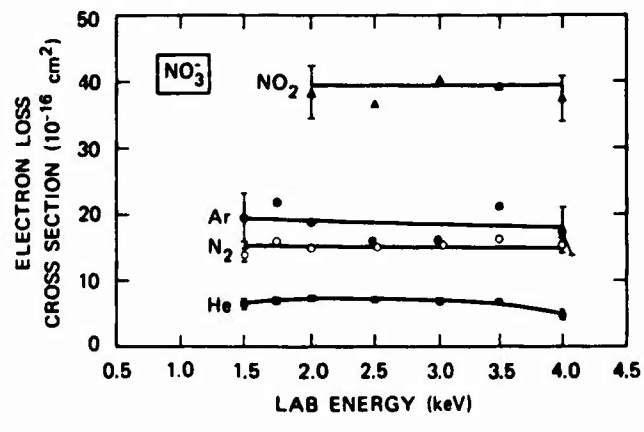

FIG. 6. Electron loss cross sections for NO_3^-.

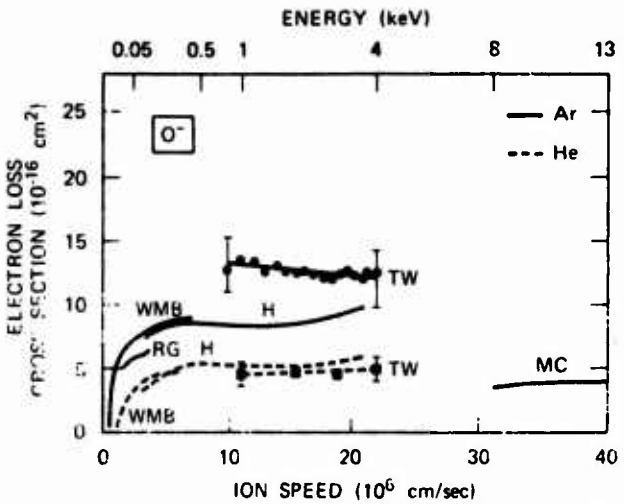

FIG. 7. O^- electron loss cross sections in He and Ar. TW = this work. H = Hasted.[6] WMB = Wynn, Martin, and Bailey.[7] RG = Roche and Goodyear,[8] MC = Matić and Čobić.[5]

charge transfer data of Mathis and Snow[12] for $O^- + O_2$ are similar to those of Snow, Rundel, and Geballe[13] and are indicated in Fig. 8. These data suggest that the collisional detachment cross section for $O^- + O_2$ is about constant at 15×10^{-16} cm^2 between 1 and 4 keV.

The only reported electron loss measurements for O_2^- are those by WMB[7] for the case $O_2^- + He$. Their results reach only as high as 400 eV, but the apparent asymptotic limit of their data agrees well with what we find at higher energies.

We know of no previous measurements of electron loss cross sections for NO_2^- and NO_3^- in this energy range. However, Ranjan and Goodyear[11] have measured collisional detachment cross sections for these ions in nitrogen and oxygen at energies below 100 eV. In each case, the cross section values are well below our higher energy results, but are still increasing at 100 eV. At their lower energies, there appears to be a correlation between the magnitude of the cross section and the negative ion electron attachment energy.

NO_3^- is known to exist in two isomers with electron attachment energies of about 2.4 and 3.9 eV.[14] The less stable "excited" NO_3^- is formed by the association of an O_2^- with a NO molecule in reactions such as $O_4^- + NO \rightarrow O_2 + NO \cdot O_2^-$, and the more stable "ground state" NO_3^- is formed in reactions such as $NO_2^- + NO_2 \rightarrow NO_3^- + NO$. We formed NO_3^- ions both by using a mixture of NO and O_2 and by using pure NO_2 in our ion source. Mixtures of all three gases were also used. Under no condition was there either an observable departure of the attenuation curve from a straight line or a dependence of the electron loss cross section on the gases used to produce the NO_3^-. Since it is likely that the NO_3^- produced in an NO/O_2 mixture would be primarily the less stable form and that the NO_3^- produced in NO_2 would be primarily the ground state form, the electron loss cross section appears to be nearly the same for the two forms of NO_3^-. This is consistent with the apparent lack of any strong correlation between the magnitude of the loss cross section and the negative ion electron attachment energy among the other reactions of this study. However, it is also possible that the NO_3^- state populations were nearly the same in both cases.

Because this series of measurements of electron loss cross sections was peripheral to our main work on the merging beams apparatus (ion–ion mutual neutralization), the scope of the work was quite limited. Despite gaps in the reactant pairs, as Table I reveals, the results of this work lend weight to ideas concerning mechanisms of collisional detachment of electrons from negative ions. In all reactions studied here, the cross sections are essentially independent of incident ion energies for the range 1–4 keV (laboratory energy) except for $O^- + O_2$ for which charge transfer is clearly important. These energies are well above threshold for detachment, but the incident ion speeds are always less than 2×10^7 cm/sec. This is below the range of validity of the theories[15–17] that treat the collision $A^- + B \rightarrow A + B + e^-$ as the scattering of a loosely bound electron moving at the speed of the incident ion. At the incident ion speeds in our studies, we would expect some form of the quasimolecular model[18–21] to apply. In this model, proposed for atomic collisions by Bydin and Dukelskii,[18] the potential curves for the ground state AB^- make a pseudocrossing with the ground state potential curve of AB at some internuclear separation R_x. If the colliding particles approach closer than R_x the electron can be ejected with some probability P which may depend on the incident ion energy and the potentials. The detachment cross section can then be expressed as

$$Q = P(R_x, W)\pi R_x^2 [1 - V(R_x)/W], \qquad (2)$$

where the projectile and target masses are M_1 and M_2, respectively, W is related to the projectile ion kinetic energy T by $W = M_2 T/(M_1 + M_2)$, and $V(R_x)$ is the potential energy of the system at the crossing distance R_x.

In the energy range of our experiments, $W \gg V(R_x)$ and Eq. (2) reduces to $Q = P\pi R_x^2$. While it is possible to determine $P(W)$ and R_x for some systems,[18,19] the

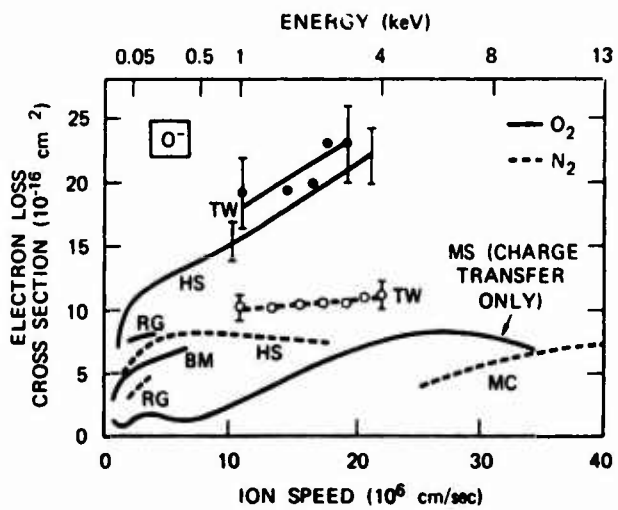

FIG. 8. O^- electron loss cross sections in N_2 and O_2. TW = this work. HS = Hasted and Smith.[6] MC = Matić and Čobić.[5] BM = Bailey and Mahadevan.[10] RG = Ranjan and Goodyear.[11] MS (charge transfer only) = Mathis and Snow.[12]

insensitivity of our cross sections to energy suggests that P is essentially constant in our energy range. Apparently if the collision energy is well above threshold, the electron is ejected with unit probability when the internuclear separation becomes smaller than a certain value. The cross section thus shows no dependence on energy. This model will hold until the collisional velocities become so large that the quasimolecular model is no longer valid. The general increase of Q with projectile and target size seen in Table I is consistent with this model. The energy dependence of Q for $O^- + O_2$ is due to the charge exchange channel. This channel is also possible in NO_2, but a strong energy dependence of Q is not evident there. Finally, there appears to be no systematic dependence on negative ion electron attachment energy for the cases studied here.

*Work supported by Defense Nuclear Agency under the technical cognizance of the Air Force Cambridge Research Laboratories.

†Present address: Chemistry Division, Argonne National Laboratory, Argonne, IL 60439.

[1]J. T. Moseley, W. H. Aberth, and J. R. Peterson, J. Geophys. Res. 77, 255 (1972), and references therein.
[2]B. R. Turner, J. A. Rutherford, and D. M. J. Compton, J. Chem. Phys. 48, 1602 (1968).
[3]R. F. Mathis, B. R. Turner, and J. A. Rutherford, J. Chem. Phys. 49, 2051 (1968).
[4]J. S. Risley and R. Geballe, Phys. Rev. A 9, 2485 (1974).
[5]M. Matić and B. Cobić, J. Phys. B 4, 111 (1971).
[6]J. B. Hasted, Proc. R. Soc. A 212, 235 (1952).
[7]M. J. Wynn, J. D. Martin, and T. L. Bailey, J. Chem. Phys. 52, 191 (1970).
[8]A. E. Roche and C. C. Goodyear, J. Phys. B 2, 191 (1969).
[9]J. B. Hasted and R. A. Smith, Proc. R. Soc. A 235, 349 (1956).
[10]T. L. Bailey and P. Mahadevan, J. Chem. Phys. 52, 179 (1970).
[11]R. Ranjan and C. C. Goodyear, J. Phys. B 6, 1070 (1973).
[12]R. F. Mathis and W. R. Snow, J. Chem. Phys. 61, 4274 (1974).
[13]W. R. Snow, R. D. Rundel, and R. Geballe, Phys. Rev. 178, 228 (1969).
[14]E. E. Ferguson, D. B. Dunkin, and F. C. Fehsenfeld, J Chem. Phys. 57, 1459 (1974).
[15]B. M. Smirnov and O. B. Firsov, Zh. Eksp. Teor. Fiz. 47, 232 (1964) [Sov. Phys.—JETP 20, 156 (1965)].
[16]G. B. Lopantseva and O. B. Firsov, Zh. Eksp. Teor. Fiz. 50, 975 (1966) [Sov. Phys.—JETP 23, 648 (1966)].
[17]D. R. Bates and J. C. G. Walker. Proc. Phys. Soc. Lond. 90, 333 (1967).
[18]Yu. F. Bydin and V. M. Dukelskii, Zh. Eksp. Teor. Fiz. 31, 569 (1956) [Sov. Phys.—JETP 4, 474 (1957)].
[19]E. A. Mason and J. T. Vanderlice, J. Chem. Phys. 28, 253 (1958); and J. Chem. Phys. 28, 1070 (1958).
[20]Yu. N. Demkov, Zh. Eksp. Teor. Fiz. 46, 1126 (1964) [Sov. Phys.—JETP 19, 762 (1974)]; and Zh. Eksp. Teor. Fiz. 49, 885 (1965) [Sov. Phys.—JETP 22, 615 (1966)].
[21]Yu. N. Demkov, G. F. Drukarev, and V. V. Kuchinskii, Zh. Eksp. Teor. Fiz. 58, 944 (1970) [Sov. Phys.—JETP 31, 509 (1970)].

APPENDIX C

CASE STUDIES IN ATOMIC PHYSICS 5 (1975) 1–45. NORTH-HOLLAND PUBL. Co.

ION–ION MUTUAL NEUTRALIZATION

J.T. MOSELEY, R.E. OLSON and J.R. PETERSON
Stanford Research Institute, Menlo Park, California, USA

Received 1 March 1974

Contents:

1. Introduction	3
2. Experimental techniques	5
2.1. Measurement of ion density decay	5
2.2. Merged beams	8
2.3. Inclined beams	12
2.4. Discussion of experimental techniques	13
3. Curve crossing model for ion–ion mutual neutralization	14
3.1. Introduction	14
3.2. Landau–Zener theory	15
3.3. Theoretical difficulties	18
3.4. Close-coupled calculations	20
4. Atomic ion systems	20
4.1. $H^+ + H^-$	20
4.2. $N^+ + O^-$, $O^+ + O^-$	23
4.3. $He^+ + H^-$, $He^+ + D^-$	24
4.4. $Na^+ + O^-$	25
4.5. Thermal energy reaction rate coefficients	29
4.6. Discussion	29
5. Cross section calculations for molecular systems	30
6. Simple molecular systems	34
6.1. $H_2^+ + D^-$	34
6.2. $NO^+ + O^-$, $O_2^+ + O^-$	34

Single orders for this issue

CASE STUDIES IN ATOMIC PHYSICS 5, no. 1 (1975) 1–45.

Copies of this issue may be obtained at the price given below. All orders should be sent directly to the Publisher. Orders must be accompanied by check.

Single issue price Dfl. 20.–, postage included.

CASE STUDIES IN ATOMIC PHYSICS 5 (1975) 1–45. NORTH-HOLLAND PUBL. CO.

6.3. $I_2^+ + I^-$ 37
7. Complex molecular systems 37
7.1. Neutralization with O_2^- 38
7.2. Neutralization with NO_2^- 38
7.3. Neutralization with NO_3^- 39
7.4. Discussion of molecular ion reactions 40
7.5. Hydrated ions 42
8. Concluding remarks 43
Acknowledgments 43
References 44

1. Introduction

The two-body ion–ion mutual neutralization reaction

$$A^+ + B^- \rightarrow A + B \qquad (1)$$

is an interesting and unusual member of the large family of electron capture (charge transfer) reactions. It is of theoretical interest because it has certain simplifying characteristics compared to most ion–neutral reactions. It is of practical interest because it occurs in any ionized gas where negative ions are formed and thus has important effects in electrical discharges, flames, lasers, and in the earth's ionosphere. In the last ten years considerable effort has been given to measurements of cross sections and rates for these reactions, and to improving the theoretical methods of treating them. This paper is intended to review the results of the various experimental and theoretical methods that have been employed to date, and will also indicate some problem areas that are not yet adequately understood.

The basic reaction is written as (1), with the understanding that the letters A and B represent either atoms or molecules. A most important physical characteristic of the reaction is that the two reactant ions A^+ and B^- are initially under the influence of the Coulomb potential, whose strong, long range attractive force leads to very large reaction cross sections (exceeding 10^{-12} cm^2) at thermal energies. A second important characteristic is that the reactions are generally exoergic and usually leave one of the products electronically excited, which can produce radiation. If the excited product is a molecule, it may be in an unbound, dissociating state and yield other fragment products.

Early experimental interest in two-body ion–ion neutralization was connected with understanding electron and ion densities in electronegative discharges [1] and flames [2]. However, the major efforts both theoretical and experimental have been stimulated by the importance of the reaction in the D-region of the earth's ionosphere [3–8]. At altitudes of 60–90 km, electrons are produced in the daytime by photoionization. These electrons may be removed either by dissociative recombination such as

$$e + NO^+ \rightarrow N + O \tag{2}$$

or by forming a negative ion in attachment reactions, either three body

$$e + O + M \rightarrow O^- + M \tag{3}$$

or dissociative

$$e + O_3 \rightarrow O^- + O_2 . \tag{4}$$

Following attachment, a number of negative ion–molecule reactions may take place to change the nature of the negative ion before the attached electron is finally returned to a positive ion. During the daytime, photodetachment reactions such as

$$O^- + h\nu \rightarrow O + e \tag{5}$$

and photodissociation reactions such as

$$CO_3^- + h\nu \rightarrow CO_2 + O^- \tag{6}$$

may very likely occur before reactions (1) removes the negative ion, starting different parts of the chain of reactions over again. More recently it has been found [9] that below 75 km and also at higher altitudes under quiescent conditions, especially at night, both the positive and negative ions are likely to undergo hydration reactions such as

$$NO_2^- + H_2O + M \rightarrow NO_2^- \cdot H_2O + M . \tag{7}$$

Subsequent clustering reactions add further water molecules, and other reactions switch the original parent ions, so that ions eventually evolve into combinations such as $H_3O^+ \cdot (H_2O)_n$ and $NO_3^- \cdot (H_2O)_n$, whose characteristics are far removed from those of the original ions. On the other hand, during disturbed conditions, such as in aurorae, the ions tend to retain a simple, unclustered character [10].

The inverse of reaction (1),

$$A + B \rightarrow A^+ + B^- \tag{8}$$

cannot easily be studied because the neutral products of (1) are generally left in excited states, and laboratory measurements of (8) must usually be made with the initial neutral species A and B in their ground states. The production of H^- in (ground state) H + Mg collisions has been studied at collision energies above 5 keV [11], and cross sections for $O + Cs \rightarrow O^- + Cs^+$ have been measured in the energy range 180–

1600 eV [12]. Differential cross sections for $Na + I \rightarrow Na^+ + I^-$ have been measured at energies from 13 to 85 eV [13]. Several studies have also been made of reactions such as $A + BC \rightarrow AB^+ + C^-$, but these are even farther removed from the true inverse of (1).

Theoretical interest in the ion–ion neutralization reaction was originally due to its simplicity among heavy particle inelastic collisions that can be understood in terms of the crossing of potential energy curves [14]. The curve-crossing model was first proposed in 1932 by Landau [15], Zener [16] and Stückelberg [17], and is commonly referred to as the Landau–Zener (LZ) theory. It has been employed extensively in recent years in theoretical treatments of collisions in which electronic transitions occur. The simplifying aspect of reaction (1) in the LZ theory stems from the fact that the initial state of the reaction (1), pertaining to the reactants $A^+ + B^-$, is Coulombic and the potential energy is well defined at large internuclear separations R, by $V(R) = -e^2/R$.

In zeroth-order approximation, ignoring interactions between electronic states, this Coulomb potential is intersected by a number of potentials of excited covalent states of the molecule AB, which are essentially flat. Thus the positions of the crossings and the slopes of the zeroth-order curves at the intersections are easily obtained. These quantities enter directly into the Landau–Zener (LZ) theory, and the simplicity in obtaining them for reactions of type (1) is attractive from the theorists' standpoint. The various theoretical treatments will be described in detail later in sections 3 and 5.

Ion–ion mutual neutralization has been reviewed briefly by Sayers [18] and Bates [19]. In a recent article in this series [20], Bates discusses the general topic of recombination, with emphasis on the historical development, applications and theory. Mahan [21] has also treated the general case of recombination of gaseous ions, including three-body ("Thomson") recombination $A^+ + B^- + M \rightarrow (A + B) + M$. Flannery [22] has made a definitive review of the theory of three-body ion–ion recombination. For a treatment of all of these and related areas the reader is referred to the comprehensive books *Collision Phenomena in Ionized Gases* by McDaniel [23] and *Electronic and Ionic Impact Phenomena* by Massey, Burhop and Gilbody [24].

In this article we deal only with the two-body reactions, with the goal of presenting a reasonably thorough picture of it as a two-body inelastic charge transfer reaction. We shall review the various experimental and theoretical studies that have been made, in an attempt to understand the physics of the reactions as well as to obtain reliable rate constants that are required for various applications in ionized gases.

2. Experimental techniques

2.1. Measurement of ion density decay

The first approaches to ion–ion recombination studies involved determinations

of the rates of decay of ion densities in reaction chambers following some form of ionization process. In an ideal case, the ion densities are monitored for a period of time after all of the initially free electrons in the volume have been removed by attachment or recombination, and under conditions such that the spatial distributions of the ions are uniform and no other loss mechanism exists except ion–ion neutralization (either two or three body). Also, ideally only one molecular or atomic form of either positive or negative ion is present in the volume, so that the ion identities are known and only one reaction is involved. Under these conditions space charge neutrality requires that the positive and negative ion densities ρ^+ and ρ^- are equal. Then the rate of change of either is given by

$$d\rho/dt = -\alpha\rho^2 , \tag{9}$$

and the ion densities themselves have time dependences expressed by $\rho^{-1} = \rho_0^{-1} + \alpha t$, where ρ_0 is the density at $t = 0$ when the measurement is started. At any pressure, the reaction rate coefficient α can be obtained from the slope of a plot of ρ^{-1} versus t. In the pressure range where both two-body and three-body processes are important, the effective neutralization rate α may be expressed as $\alpha = \alpha_2 + \alpha_3$, the sum of the respective two-body and three-body rate coefficients. Three-body recombination can be viewed as the formation of an unstable complex ($A^+ + B^- \rightarrow AB^*$) which is then stabilized into AB or A + B by collision with a gas molecule. Thus the three-body rate coefficient α_3 will be linear in pressure until the pressure becomes high enough that the time between collisions approaches the lifetime of the complex AB^*, when α_3 will lose its linearity with pressure. The two-body rate α_2 can in principle be determined from the zero pressure intercept when α is plotted versus pressure, but this will be valid only when it is established that α_3 is linear with pressure. In many cases, even when α_3 is linear with pressure, α_2 may be much smaller than α_3, and the extrapolation method of determining α_2 is not very accurate.

Ion densities have been monitored by several techniques. Some of the earliest studies, by Yeung [1] and Greaves [25], utilized a measurement of the dielectric constant of the afterglow plasma following ionization by r.f. fields. Shifts in the resonant frequencies of r.f. sampling probes were the measured parameters. In a related method, Knewstubb and Sugden [2] measured the change in the Q of a resonant r.f. circuit, caused by ionization in an alkali water-vapor flame. They associated this shift with the electrical conductivity and thus determined the ion densities. Recently, a more sophisticated experiment by Eisner and Hirsh [26] determined the conductivity of air-like mixtures following ionization by high energy electrons.

Most of these ion density decay measurements have been made using apparatures in which ion currents from the afterglow plasmas have been collected, usually using weak electric fields to draw the ions to collector plates, and have only determined three-body "volume" recombination coefficients at pressures above 10 torr. However, Mahan and coworkers [27–29] made extensive measurements at pressures down

to less than 10 torr, which allowed them to deduce two body recombination coefficients.

In practice, the ideal conditions listed at the start of this section never exist and the analysis required for proper interpretation of the results is very complicated. Consequently, much of the early work was improperly analyzed. In his recent review, Mahan [21] has summarized the complexities of dealing with real systems. Only a brief discussion of some of these complications will be given here.

Diffusion losses modify the loss rate equation (9) so that it becomes

$$\partial\rho/\partial t = -\alpha\rho^2 - D\nabla^2\rho \qquad (10)$$

where D is the effective diffusion coefficient which is often assumed equal for positive and negative ions. McGowan [30] analyzed diffusion effects for a plane parallel ionization chamber and applied the results to his measurements [31]. Fisk, Mahan and Parks [29] used a numerical solution to account for their diffusion effects. In addition to these diffusion losses, which can be accounted for, inhomogeneities in the initial ion densities can lead to errors in the interpretation of the decay rates.

A common problem in most experiments is that more than one ion species of each charge exists in the afterglow. In many gas mixtures, several ion–molecule and charge transfer reactions can take place before the most stable species of each is reached. Until this stabilization is reached, ion–ion neutralization occurs between several species, and the effective rate is some average of the individual rates. Since the diffusion coefficients may be different for each species, the analysis becomes difficult. Mass analysis has been used to sample the ions in the more reliable experiments. Thus, Greaves [25] was able to identify $I_2^+ + I^-$ as the only reacting pair in his chamber. Similarly, Fisk, Mahan and Parks [29] identified their reactants as $Tl^+ + I^-$, $Tl^+ + Cl^-$, $Tl^+ + Br^-$ only, in pure vapors of TlI, TlCl and TlBr, respectively, at low pressure, while at higher pressures (and temperatures), the dominant ions become Tl_2I^+ and TlI_2^-, etc. On the other hand, mixtures of TlI and NO_2 produced a complicated spectrum whose effective recombination coefficients were not easily interpretable. Mass sampling provides a clear interpretation when only one reaction is controlling the ion decay, but the results become less useful when a variety of ions is found.

In examining air-like mixtures that contained several ions of each charge, whose relative densities depend on the length of time since irradiation by 1 MeV electrons, Hirsh and Eisner [26, 32] used a theoretical model to obtain rate coefficients from their mass spectrometer data. Ions were sampled from air-like mixtures at 2–22 torr following bombardment by 1 MeV electrons. A varying number of ions of several species were found, whose relative populations depended on the gas mixture, length of irradiation time, and pressure. The theoretical model was used to deduce two-body neutralization rates for $NO^+ + NO_2^-$ and $NO^+ + NO_3^-$ from the sampled ion current data. Total ion density decay rates were determined from plasma conductivity measurements using an r.f. probe. This technique is particularly appealing for

studies of atmospheric ion species because it can approximate some of the conditions that must exist for the natural formation of these ions. However, proper data analysis requires a model that must account for different diffusion rates, wall effects, and possibly competing reactions. An accurate model can thus become very complicated, and tests of its validity are difficult. Since the early measurements of Eisner and Hirsh [26], the model has been further advanced [33].

2.2. Merged beams

In order to overcome some of the uncertainties inherent in most bulk measurements of ion densities described in the previous sections, the more complicated "merged beams" method was developed for ion–ion reactions at Stanford Research Institute [34, 35]. In this method, two mass-selected ion beams moving in the same direction are superimposed over a known path length, and then separated. The ions each travel at high speeds in the laboratory frame of reference, with kinetic energies of several keV, but the relative speeds in the center of mass frame can be made very small, approaching thermal velocities. The identities of the ions can be established, and the relative collision energies can be accurately controlled over a wide range. Thus, the cross section energy dependence as well as its absolute magnitude can be established, providing more insight into the details of the electron transfer reactions than is possible by bulk measurements.

The merged beam technique was first used to study ion–neutral reactions and has been reviewed by Neynaber [36]. In addition to the advantage of mass selection, the technique offers a very precise determination of the relative kinetic energies of the colliding ions, as may be seen from the following brief analysis.

The relative energy E_r of ions in two beams traveling at speeds v_1 and v_2 in the laboratory and at an angle θ with respect to each other is

$$E_r = \tfrac{1}{2}\mu v_r^2 = \tfrac{1}{2}\mu(v_1^2 + v_2^2 - 2v_1 v_2 \cos\theta), \tag{11}$$

where μ is the reduced mass. In a merged beams apparatus, ideally $\theta = 0$ and the relative energy E_{ro} is given by

$$E_{ro} = \tfrac{1}{2}\mu(v_1 - v_2)^2 = \mu[(E_1/M_1)^{\frac{1}{2}} - (E_2/M_2)^{\frac{1}{2}}]^2 \tag{12}$$

where E_i and M_i refer to the laboratory energy and mass of each ion. The precision in the relative energies results from a "deamplification" in transforming the laboratory energies into the relative (center of mass) collision energies. This effect is easily seen in the case of equal masses $m_1 = m_2$ and small energy differences $\Delta E = E_2 - E_1$. In this case eq. (12) reduces to $E_r \approx (\Delta E)^2/8E$, where E is the mean lab energy. A similar deamplification in the general case reduces the normal energy spreads of a few eV in each of the beams to very small amounts in the center-of-mass system. In fact, in a practical experiment, when the average relative energy is in the range below 1 eV, the greatest uncertainty in the relative energies is due to imperfect alignment and col-

limation of the beams [35, 37]. This effect can be understood with the aid of eq. (11), where θ represents the angle between any two colliding ions. When θ is small, eq. (11) becomes

$$E_r \approx \tfrac{1}{2}\mu[(v_1 - v_2)^2 + v_1 v_2 \theta^2] = E_{ro} + \mu(E_1 E_2/m_1 m_2)^{\frac{1}{2}}\theta^2 . \quad (13)$$

E_{ro} is the relative energy of the two beams determined from the difference in the laboratory energies, as one would obtain from eq. (12). Thus, because of the transverse velocity components, the average energy is increased, and an uncertainty in θ produces an uncertainty in E_r. Practical lower limits to E_r are generally near 0.1 eV.

The original apparatus at Stanford Research Institute (SRI) [34, 35] has undergone several internal modifications, and is presently in a form represented schematically in fig. 1. The two beams are generated in duoplasmatron ion sources, mass-selected in Wien-type $E \times B$ velocity filters, focused, and merged in a common magnet. The superimposed beams then enter an ultra-high vacuum chamber and flow together over the interaction path until they are separated by electrostatic deflection (at "Demerger B" in fig. 1) and finally collected for current measurement. The fast neutral particles formed from the beams along the interaction path continue undeflected until they are stopped and detected by secondary electron emission. Complete collection is possible because all reaction products are in a narrow cone surrounding the beam axis.

The pressure in the interaction chamber is maintained below 2×10^{-9} torr during the experiments by titanium sublimation pumping, backed by an oil diffusion pump (the ultimate pressure with beams off is about 5×10^{-10} torr). However, even at 2×10^{-9} torr, the fast neutrals in the beam produced by charge trans-

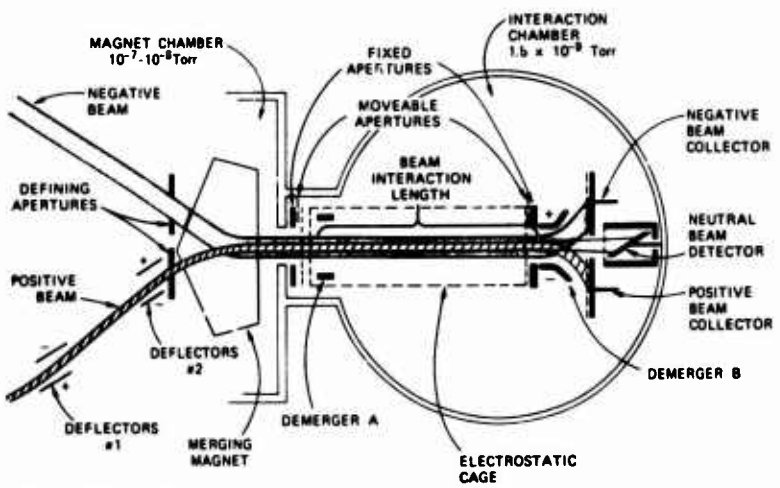

Fig. 1. Schematic of the merged beams apparatus at Stanford Research Institute.

fer ($A^+ + G \rightarrow A + G^+$) and collisional detachment ($B^- + G \rightarrow B + G + e$) reactions with the background gas (G) outnumber the ion–ion neutralization products by one or two orders of magnitude. In order to eliminate these beam–gas contributions from the neutral product signal, the two beams are chopped at different rates and the signal is coherently detected at the difference frequency [35].

To define the interaction path length, and to eliminate the interference signal which arises from beam–beam interactions as the beams are being merged in the magnet chamber, the beams may also be separated by a pair of plates ("Demerger A") located just inside the interaction chamber. The effective interaction path length is thus the distance between the demergers (33 cm).

Changes in relative energies are made in two ways. Small changes over a limited range are easily made by changing the potential on an electrostatic cage which surrounds the merged beams over the path between the two sets of deflection plates. A pair of high transparency plane-parallel grids, oriented perpendicularly to the beam path, is located just in front of the cage. One grid is electrically attached to the electrostatic cage and forms the entrace "window" to the cage. The other is ground and is located about 0.5 cm ahead of the cage. Thus, only the uniform field between the grids is experienced by the ions as they enter the cage. A potential V_c on the cage will change the relative laboratory energies by $2V_c$. In practice, potentials of up to ± 400 V can generally be used without seriously affecting the beam trajectories, allowing a relative energy range of order of 10–50 eV to be easily covered. Other sets of energies can be covered by changing one of the main beam energies, which requires changing its entrance angle at the magnet in order that it have the same exit angle as the other beam. This may be done either [35] by changing the angle of the appropriate ion source chamber (both are rotatable about the center of the magnet), or by using two sets of deflectors [38] located in front of the merging magnet, labeled "Deflectors" 1 and 2 in fig. 1. Once the beam's energy is changed and the beam is realigned, the electrostatic cage potential may be varied to cover a new, partially overlapping, range of relative energies. The ability to cover the same relative energy with more than one laboratory beam energy and entrance angle affords a check on the reliability of the data.

Proper beam focusing and adjustment require great care. The neutral product signal depends [35] on the beam current density overlap integral $\int J^+ J^- \mathrm{d}V$, where the J's represent the current densities and the integral is taken over all the volume V common to the two beams along the interaction path. Focusing, adjustment, and an approximate solution to the overlap integral are facilitated with the use of two movable beam flags containing small apertures, each 0.3 cm in diameter. These can be moved accurately into position centered on the beam axis at each end of the interaction path next to the larger, fixed 1.3 cm diameter apertures at each end, as described in [35] and [39].

The signal also depends on the average secondary electron emission coefficients γ appropriate to the fast neutral products that strike the neutral product detector. This detector is a stainless steel plate, oriented at 45° to the beam direction in order

to increase the secondary electron yield. The secondary electron currents that flow from this plate to the walls of the surrounding detector enclosure, which are biased at a positive voltage, provide the neutral product signal. The value assigned to γ is the average of γ^+ and γ^-, the coefficients corresponding to the two ion beams, which are measured frequently during the experiments. This method of determining γ, and its reliability, are discussed in [39]. It is regarded to be accurate to within 10% of the actual effective γ of the neutral products, direct measurement of which is experimentally inaccessible.

In order to reach minimum energies, the average laboratory speeds of the two beams must be made equal. Under this condition the momenta of the positive and negative ions are proportional to the respective masses, and the angles through which the beams are deflected in the common merging magnet are roughly inversely proportional to the ion masses. Thus, the heavier ion is deflected less than the lighter ion, and correspondingly less mass (momentum) selection is afforded the heavier ion. In most cases several ions of the same charge may exist in the beam produced by the ion source, and often the merging magnet does not provide adequate mass selection. As a result, Wein $\boldsymbol{E} \times \boldsymbol{B}$ velocity filters were installed along each beam path to provide primary mass selection.

Although the average laboratory speeds in the two beams may be equal, the lower limit to the effective relative energy in the beams is non-zero, due to velocity components transverse to the beam direction stemming from incomplete collimation and imperfect focusing (see eq. (13)). In the SRI apparatus, the lower limit to the center-of-mass energy is in the range 0.1–0.2 eV due to these effects.

The total energy range covered in most measurements extends from about 0.15 eV to about 200 eV. This large dynamic range has aided the development and testing of fairly effective but still uncomplicated theoretical models for both atomic ions [40,41] and molecules [42]. However, more accurate theories will require further refined measurements of final states since only total cross sections have been subject to extensive study.

In order to predict thermal reaction rates, which are required for applications in aeronomy, the SRI group has used an extrapolation technique to extend their measured cross sections to lower energies [37–39]. This technique will be discussed in section 3.

A different configuration of a merged beams apparatus has been used by Weiner, Peatman and Berry [43,44] at the University of Chicago to study optical emissions from the final states of $Na^+ + O^-$ neutralization reactions. Figure 2 is a schematic drawing of that apparatus. Here each ion beam is deflected through 180° in the merging magnet. Photons can be observed through two windows, one on the top and one on the side of the vacuum chamber. Interference filters are used to select the desired emission line, and the light is focused by a lens onto a photomultiplier. Individual photons are counted and a sequence of beam-chopping and count-gating pulses permits various background counts to be subtracted from the total photon counts. The signal to noise ratio is about 0.1.

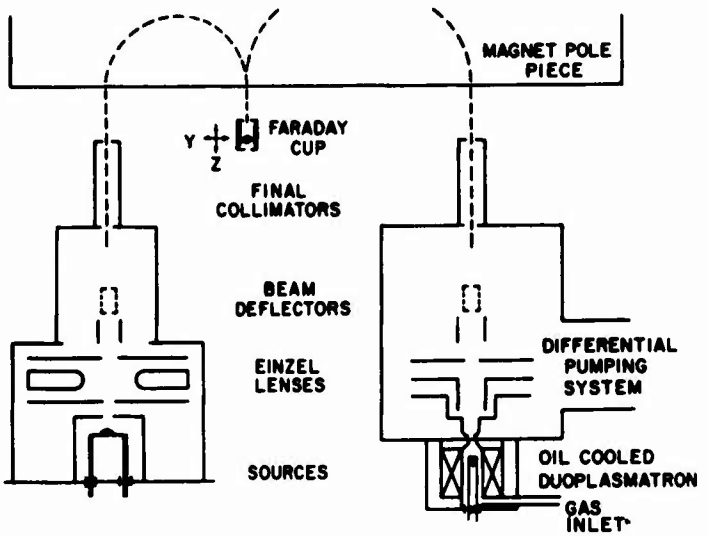

Fig. 2. Schematic of the merged beams apparatus of Weiner, Peatman and Berry [43,44].

The primary difficulty in obtaining absolute neutralization cross sections from this experiment is calibration of the sensitivity of the photon detection system. The optical collection efficiency is estimated geometrically, and the single photon counting efficiency of the photomultiplier is assumed to be the same as the quantum efficiency quoted by the manufacturer. It has recently been shown [45] that these quantities can differ substantially. Therefore the uncertainty in the photon counting sensitivity is difficult to assess, and the absolute value of the cross sections determined by this experiment are subject to some question.

Since this experiment observes optical emission from the neutral products of an ion–ion neutralization reaction, it provides direct information about the final states of these reactions and the energy dependences of the various reaction channels. Thus important new information can be made available for the theoretical understanding of the collision processes, and, as will be discussed in section 4, some surprising results have been obtained.

2.3. Inclined beams

The first measurements of one of the most theoretically interesting ion–ion neutralization reactions, $H^+ + H^- \rightarrow H + H$, were performed by Rundel, Aitken and Harrison [46] and by Gailey and Harrison [47] at the United Kingdom Atomic Energy Authority Laboratory in Culham, England, using an "inclined beams"

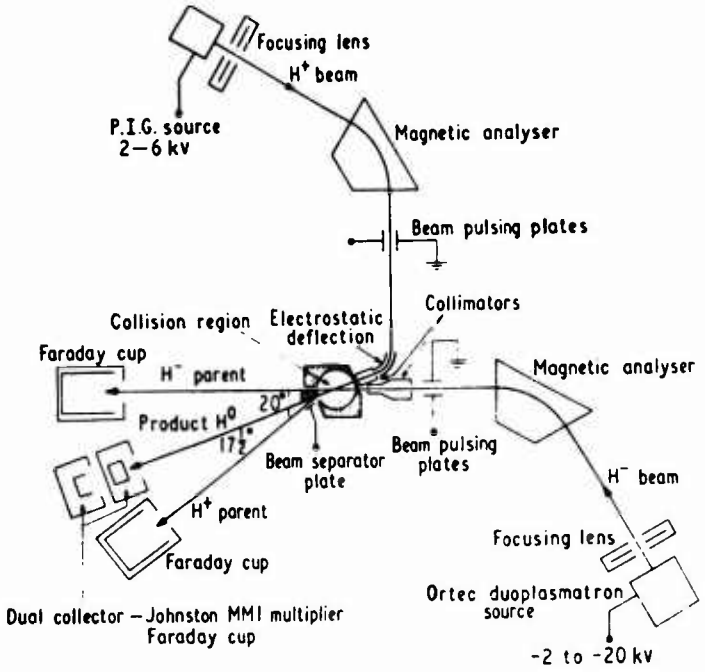

Fig. 3. Schematic of the inclined beams apparatus of Harrison and co-workers [46–48].

technique. A schematic of their apparatus is shown in fig. 3. The positive and negative beams intersect each other at an included angle θ (see eq. (11)) of 20°. Following the collision region, the proton beam is further deflected into a Faraday cup, while neutrals formed proton interactions with the H^- beam and the background gas continue into the neutral detector. Chopping of both beams is employed to allow subtraction of background effects.

While this technique does not permit measurements at nearly thermal relative energies, as in the merged-beams methods when $\theta = 0°$, it does allow the energy range to be extended to much higher energies. Thus the $H^+ + H^-$ studies were carried out at large center of mass energies, between 125 and 5000 eV. At these relatively high energies it is important to separate the products from the $H^+ + H^-$ collision since electron detachment, $H^+ + H^- \rightarrow H^+ + H + e$, becomes increasingly likely. By observing only neutrals formed from the positive beam, this experiment measures the ion–ion mutual neutralization cross section without possible interference from electron detachment. This apparatus was also used to make measurements on $He^+ + H^-$ [48], which was also studied at SRI [40].

2.4. Discussion of experimental techniques

The three basic techniques that have been used to study ion–ion neutralization

are complementary. The bulk gas techniques allow measurements to be made at thermal energy between ions that are in most cases likely to be in their ground states. In order to unambiguously determine the reaction rate for a particular pair of ions, however, it is generally necessary to use a mass analyzer. Even then, analysis becomes very complex if more than two species of ions are present.

The merged beams technique allows measurements on well identified pairs of ions over a wide energy range (0.1 to several hundred eV). Absolute cross sections can be measured as a function of energy, and by observing optical emission the final neutral states can be investigated. Absolute accuracy is so far limited to about 30%, mainly by the difficulty in determining the overlaps of the ion beams, and is even further restricted when photon measurements are used. Further, for molecular ions, uncertainty in the vibrational and electronic states of the interacting ions leads to some ambiguity in the results, as will be discussed in more detail later.

The inclined beams techniques (as well as any other "crossed beam" measurement) has similar advantages and disadvantages to the merged beams technique. It cannot approach the low energy limits of the merged beams but can distinguish between neutral products from the positive and negative beams.

3. Curve crossing model for ion–ion mutual neutralization

3.1. Introduction

A theoretical model that has been used with some success to calculate the ion–ion mutual neutralization total cross section is the Landau–Zener [15–17] curve crossing theory. A general description of the application of this model to the ion–ion neutralization problem was first given by Bates and Massey [14] and subsequently reviewed by Massey [49]. Later, Magee [50] applied the Landau–Zener theory to the multicrossing case of $O^+ + M^- \rightarrow O + M$ where M was O and O_2.

This theoretical approach can be discussed with the aid of fig. 4. For this discussion it will be assumed that both ions are atomic. The initial state of the system is $(A^+ + B^-)$ at internuclear separation $R = \infty$. If the ions approached each other without interacting except through the Coulomb force, the potential energy of the system would follow the Coulomb potential curve $-e^2/R$. In fig. 4 this Coulomb curve is "crossed" by those of several excited neutral states. These neutral state curves approach $R = 0$ horizontally until A and B begin to interact at close separations, usually about 4 to 6 atomic units. Consider the crossing labeled "2" in fig. 4. As $(A^+ + B^-)$ approaches such a crossing with a neutral state (A + B) of the same symmetry, an interaction between the states can occur, which causes an actual crossing to be avoided, as indicated. During the collision, as R decreases past the crossing distance R_x, the system has some probability p of making a transition to the other state. This same probability exists as the collision partners separate. The theories of Landau [15], Zener [16] and Stueckelberg [17] provide a way of calculating this probability, which will be discussed later in this section. For a single crossing such as "2," the probability P of a transition from $(A^+ + B^-)$ to (A + B) is $P =$

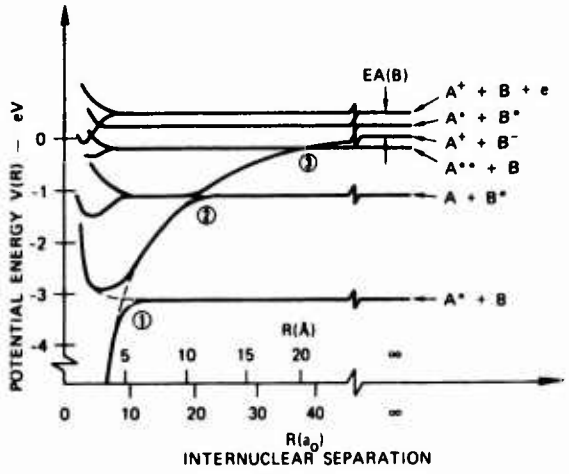

Fig. 4. Simplified potential energy curves for a "typical" atomic ion system.

$2p(1-p)$, and the result for multiple crossings follows logically.

The ion–ion neutralization reaction is appealing theoretically because it offers the simplest test of the LZ theory. The crossing points and the difference in slopes of the two non-interacting curves at the crossing, which are needed to calculate the transition probability, can be accurately determined since the Coulomb curve is known and the neutral potentials are essentially flat.

3.2. Landau–Zener theory

The transition probability for a crossing between an initial state i and a final state f is given by the Landau–Zener model [15–17] as*

$$p_{if} = \exp(-2v_x/v_b) \tag{14}$$

where v_b is the radial velocity for impact parameter b at the crossing point R_x, and

$$v_x = \pi H_{if}^2(R_x)/|V_i' - V_f'| . \tag{15}$$

In eq. (15) V_i and V_f are the initial and final state potentials, respectively, H_{if} is the coupling matrix element between the states, and V_i' is dV_i/dR evaluated at R_x. The total cross section is given by

$$Q_{if} = 2\pi \int_0^{b_x} bP_{if}(b)\,db , \tag{16}$$

where the impact parameter b is related to the angular momentum l and the wave number k by

* Atomic units will be used throughout this section and section 5.

$$b = (l + \tfrac{1}{2})/k \,. \tag{17}$$

The impact parameter for the crossing point is given by

$$b_x = R_x [1 - V_i(R_x)/E]^{\frac{1}{2}} \tag{18}$$

In the special case of only one crossing, P_{if} has the form, as mentioned,

$$P_{if} = 2p_{if}(1 - p_{if}) \,. \tag{19}$$

In a multicrossing system, however, allowance must be made for the change in P_{if} due to other curve crossings [50].

For the case at hand, reaction (1),

$$A^- + B^+ \rightarrow A + B + \Delta E \,, \tag{1}$$

where A or B may each or both be in excited electronic states, the initial potential curve is Coulomb, and the final state is that of separated neutral atoms. For moderate energies, important crossings occur only over a limited range of internuclear separation R. At large distances, the coupling matrix elements die off exponentially, while for close encounters, transitions occur only at high velocities and small impact parameters, and these make only a small contribution to the total cross section. Favored crossings occur from about 10 to 50 a.u. For these separations, to a good approximation the interactions between the neutral atoms may be neglected compared to the Coulombic one. Then

$$\Delta E = -V_i(R_x) = R_x^{-1} \tag{20}$$

and

$$|V_i' - V_f'| = R_x^{-2} \,. \tag{21}$$

The value of ΔE can be calculated directly from the ionization potential of A, I.P.(A), the electron affinity of B, E.A.(B), and the levels of excitation of the neutral products, E(A), and E(B). For ground state products ΔE is given by

$$\Delta E = [\text{I.P.(A)} - \text{E.A.(B)}] \,. \tag{22}$$

In more defined treatments [51–53] of reaction (1), the polarizabilities of the initial and final states are taken into account to obtain more accurate evaluations of eqs. (20) and (21). This effect becomes very important at small crossing distances, but at the separations of importance here (10–50 a.u.) eqs. (20) and (21) are adequate. For the alkali–oxygen systems, this has been verified by van den Bos [53] and for

the $H^+ + H^-$ reaction, the values of Bates and Lewis [51] do not deviate significantly from the predictions of the above equations.

Therefore, from eqs. (15) and (21), we obtain

$$V_x = \pi R_x^2 H_{if}^2(R_x) \tag{23}$$

and from (18)

$$b_x = R_x[1 + (R_x E)^{-1}]^{\frac{1}{2}} . \tag{24}$$

The radial velocity v_b at R_x is given by

$$v_b = v[1 + (R_x E)^{-1} - (b/R_x)^2]^{\frac{1}{2}} , \tag{25}$$

where v is the incident velocity. From a knowledge of the electron affinity of A, the ionization potential of B, and the electronic energy levels of A and B, the ΔE's of reaction (1) for transitions to the various states may be calculated by eq. (22). Then, by eq. (20), the crossing point for each ΔE is known. Now all the quantities necessary for the calculation are realized, except for the coupling matrix elements.

These matrix elements are difficult quantities to obtain by *ab initio* calculations. Olson, Smith and Bauer [54] have used a semi empirical method to obtain approximate values for the H_{if}'s. A graph was set up similar to that of Bauer, Fisher and Gilmore [55] following the work of Hasted and Chong [56]. This plot included all of the then presently available R_x versus H_{if} values for one-electron transfer systems, 98 points from both experimental and theoretical work. It was found that by plotting reduced quantities the data scattered about common curve of $H_{if}^* = 2H_{if}/(\alpha \cdot \gamma)$ versus $R_x^* = \frac{1}{2}[(\alpha + \gamma)R_x]$. Here $\frac{1}{2}\alpha^2$ is the electron affinity of B, and $\frac{1}{2}\gamma^2$ is the effective ionization potential of A in eq. (1). When parameterized as

$$H_{if}^* = R_x^* \exp(-0.86 R_x^*) , \tag{26}$$

eighty-three percent of all data were within a factor of 3 of this curve. The range of H_{if}^* covered was from 10^{-1} to 10^{-10} and R_x^* from 2 to 28. Eq. (26) can thus be used to estimate H_{if}.

Another method, developed by Smirnov [57] can be used for the calculation of H_{if} in the case where the negative ion is in an S state. It is much more rigorous in nature than the semi-empirical scheme of Olson et al. [54], and employs asymptotic expansions for the wave functions of the negative ion and the excited atom. It is represented as

$$H_{if}^2 = \gamma\alpha^2 A^2 (2R_x^2)^{-1} (4/e)^{1/\gamma} (\alpha R_x)^{2/\alpha} (2l+1) \Gamma^{-1}(1/\alpha + l + 1) \times \Gamma^{-1}(1/\alpha - l) \exp[-(\alpha+\gamma)R_x] , \tag{27}$$

where α and γ have been defined previously, l is the orbital angular momentum quantum number for the electron in the excited atom, and $A^2 = 2.65$ for H^-.

At a given energy, if only two states dominate the scattering, eq. (16) may be solved in closed form by the use of tabulated integrals [51, 52]. We then find that

$$Q_{if} = 4\pi R_x^2 (1 + \Delta E/E) F_3(\lambda) , \tag{28}$$

where

$$F_3(\lambda) = \int_1^\infty e^{-\lambda z} (1 - e^{-\lambda z}) z^{-3} \, dz, \tag{29}$$

in which

$$\lambda = \frac{2v_x}{v(1 + \Delta E/E)^{1/2}} = \frac{\sqrt{2}\pi R_x^2 H_{if}^2(R_x)\mu^{1/2}}{(E + \Delta E)^{1/2}} . \tag{30}$$

$F_3(\lambda)$ is effectively an integral of the transition probabilities over all impact parameters. The important range of crossing distances, 10 to 50 a.u., corresponds to a range of ΔE of 0.02 to 0.1 a.u. or 0.5 to 3 eV. Thus at near thermal energies, E in eq. (30) becomes negligible compared to ΔE, and λ approaches a constant equal to $2^{1/2}\pi R_x^{5/2} H_{if}^2 (R_x)\mu^{1/2}$. The cross section is then domianted by a v^{-2} dependence of the form

$$Q_{if} = 4\pi R_x^2 \Delta E \, F_3(\lambda)/E = 8\pi R_x F_3(\lambda)/\mu v^2 \tag{31}$$

where $F_3(\lambda)$ is constant. This v^{-2} tendency is evident in the low energy experimental data described in the next sections.

For energies $E \lesssim \Delta E$, $F_3(\lambda)$ can be approximated by a polynomial, and Q_{if} can be parameterized as

$$Q_{if} = A/v^2 + B/v + C + Dv. \tag{32}$$

This form is useful for extrapolating merged beam data to lower energies for the purpose of obtaining thermal energy reaction rates. The monoenergetic reaction rate is $\alpha = v_r Q$, and thermal rates can be obtained by averaging over a Boltzmann distribution.

We see also from eq. (31) that at low relative velocities there will be an isotope effect when Q is plotted against v_r. At high velocities Q will depend only on v_r, for a given pair of reactants. The isotope effect will be shown later in the $He^+ + H^-$ and $He^+ + D^-$ calculations.

3.3. Theoretical difficulties

Several shortcomings of the Landau–Zener theory and the curve crossing model

presented above should be recognized. The first problem is associated with the LZ theory itself. The potentials that cross are assumed to be linear and the coupling matrix element is assumed to be constant in the region about the crossing point R_x. These approximations can lead to erroneous results if the potentials deviate significantly from linear forms. There are also problems at higher energies where the Landau–Zener theory predicts that the total cross sections will decrease as $E^{-1.2}$ instead of the correct E^{-1} dependence [58, 59]. Recently however, Dubrovskii [60] has derived a correction term for the high energy LZ dependence which remedies this difficulty. Also, the simple LZ theory as presented above does not take into proper account the possibility of tunneling through the potential barriers to allow for reaction at impact parameters whose classical turning points are at internuclear separations greater than R_x. It has been estimated [42] that this effect will cause the calculated ion–ion neutralization cross sections to be too small by approximately 10%.

Most likely, a good share of the difficulty in comparing the theoretical results to the experimental ones does not simply lie in the inadequacies of the LZ theory but in other aspects of the problem. One source of difficulty is obtaining coupling matrix elements, H_{if}, that are more accurate than a factor of two or three. This requires detailed *ab initio* potential calculations which are extremely difficult, time consuming, and costly for these types of systems. If the matrix elements are increased by a factor of three, there can for many cases be a similar increase in the calculated total cross sections, expecially for a system where there are only a few product states available and therefore few curve-crossings.

Another possible source of difficulty in previous calculations is the neglect of rotational coupling between reactant and product states of different symmetry, such as transitions between Σ and Π, or Π and Δ molecular states. For the $H^+ + H^-$ system, it has been found [61] that the inclusion of rotational coupling can have an effect on the calculated total cross sections even at thermal energies. The reason can be seen by examining the rotational coupling matrix element where L_x is the rotational coupling matrix element evaluated at R_x. If we look at the impact parameter b_x that corresponds to a turning point at R_x, eq. (24) and substitute it into eq. (33) we obtain at thermal energies

$$H_{12}(b = b_x, R_x) = vL_x[1 + (R_x E)^{-1}]^{\frac{1}{2}}/R_x \approx L_x(2/\mu R_x^3)^{\frac{1}{2}} . \tag{34}$$

Thus, if L_x is of the order of 0.1, even at thermal energies transitions caused by rotational coupling can be important for the lighter systems. Note the dependence in eq. (34) on the reduced mass of the system.

The LZ theory also cannot be expected to apply to transitions occuring when there is no curve crossing. Optical measurements performed on the $Na^+ + O^-$ system [43, 44] show an appreciable contribution to the total cross section from a product state that does not cross the Coulomb potential. This measurement indicates that these types of interactions must be considered.

Even with all the forementioned difficulties, the LZ curve crossing theory does display an energy dependence for the total cross sections that is generally in good agreement with experimental "merged-beam" results. Moreover, the predicted magnitude of the cross sections are within a factor of two of experimental results for most species.

3.3. Close-coupled calculations

The bulk of the total cross section calculations for atomic species of reaction (1) have been performed using the LZ curve-crossing model because of its ease of application. The most accurate approach, however, would be to perform numerical calculations on the coupled Schroedinger equations that described the nuclear motion. These equations must be solved for the transition probabilities of each possible product channel at every orbital angular momentum quantum number l. The probabilities are then summed to obtain the cross section. This type of calculation requires a prohibitively large amount of computer time if the number of possible channels exceeds three or four. As a result, only for one system, $H^+ + H^-$, has a calculation of this type been attempted [62]. Here, *ab initio* potential curves and coupling matrix elements were used to obtain the cross sections. These results will be presented in the next section.

One approximate close-coupled method that has not been used, but appears to be ideally suited to the ion–ion problem, is that presented by Gordon [63]. In his method, the potential curves are approximated by linear pieces so that the wavefunctions can be represented by Airy functions. The close-coupled calculation is then performed with grids equal to the sizes of the potential pieces instead of being determined by the rapid oscillation frequency of the wave functions. For the ion–ion case where the product potentials are almost linear, the method of Gordon should be very efficient for close-coupled calculations.

Classical close-coupled methods such as the one presented by Bates and Crothers [64] could also be applied to this problem. However, the difficulty with the classical methods is that an "average" trajectory must be chosen. In the case where there is more than one product channel this becomes extremely difficult for low energy collisions ($E \lesssim 100$ eV). At higher energies, however, the classical methods may be applied.

4. Atomic ion systems

4.1. $H^+ + H^-$

A relatively simple ion–ion system for comparison with theoretical calculations is $H^+ + H^-$. The cross section for this reaction has been measured over the energy range from 0.15 to 300 eV at SRI [37], and from 125 to 5000 eV by Rundel, Aitken and Harrison [46]. The results are shown in fig. 5. The two measurements are in excellent agreement where they overlap, and in combination provide a measurement

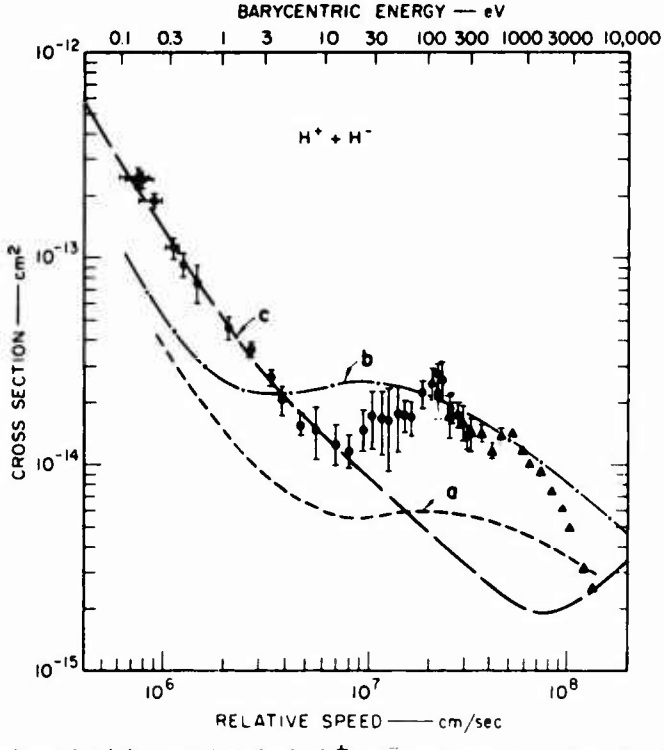

Fig. 5. Experimental and theoretical results for $H^+ + H^-$. ● - Moseley, Aberth and Peterson [37]. ▲ - Rundel, Aithen and Harrison [46], a - Bates and Lewis [51], b - Dalgarno, Victor and Blanchard [62], c - Olson, Peterson and Moseley [40].

of this cross section spanning an energy range of more than four orders of magnitude.

This system should be well suited for a test of theoretical calculations because there are only two electrons, facilitating *ab initio* calculations, and the initial and the final state potentials are well defined. The zero order potential curves for this system are given in fig. 6. A number of LZ calculations using interaction matrix elements obtained in a variety of ways, have been made on this system and the results are shown in fig. 5. The earliest calculation by Bates and Lewis [51], is given by curve "a". It has the general characteristics of the measured cross section, but is lower in magnitude by about a factor of three. The increase in the cross section at low velocities is caused by the crossing to the $n = 3$ state of H, and the maximum at higher velocity is caused by the $n = 2$ crossing. The failure of the calculation to decrease rapidly enough at high velocity is expected because of the invalidity of the LZ theory at these high energies. At high energies the LZ theory incorrectly predicts that the cross sections should decrease as $1/v$ instead of $1/v^2$.

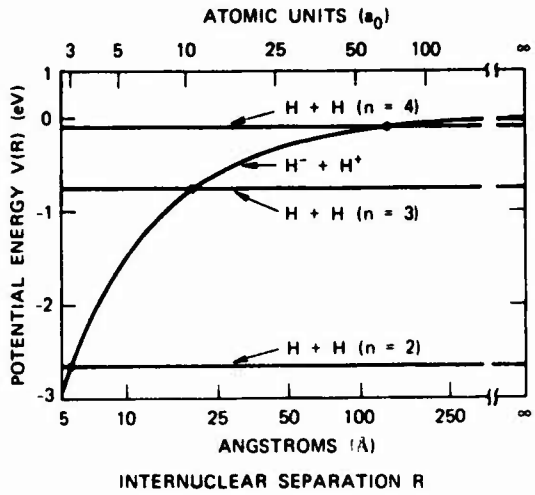

Fig. 6. Zero order potential curves for $H^+ + H^- \cdot H + H$.

Curve "b" represents the LZ calculations of Dalgarno, Victor and Blanchard [62] which were based on more accurate potential curves for the H_2 molecule. This result is nearer the measured cross section in absolute value than that of Bates and Lewis but does not reproduce the velocity dependence satisfactorily. Recently, Browne and Victor hare extended these calculations and have included rotational coupling between initial and final states. They found [61] that the calculated cross sections are increased substantially. Apparently, rotational coupling will have to be included in any detailed calculation on an ion–ion neutralization system.

Curve "c" represents the LZ calculation of Olson et al. [40] using interaction matrix elements calculated by the method of Smirnov [57]. This calculation compares quite favorably with the experimental results below 10 eV, but departs from them significantly at higher energies. The Smirnov formula was derived using asymptotic wave functions, and therefore it would be expected that interaction matrix elements for crossings at large distances would be more accurate than those for smaller distances. Clearly the $n = 3$ crossing at $R_x \approx 36$ a.u. is much better represented than the $n = 2$ crossing at $R_x \approx 10$ a.u.

Recently, Janev and Tancic [65] have calculated the $H^+ + H^-$ cross section, using the technique of Dubrovskii [55]. These results indicate extremely good agreement with experiment. However, it appears there is a numerical error in the partial cross section arising from the $n = 2$ state so that the high energy cross section calculations are too large by approximately a factor of 3.

It thus appears the LZ calculations are able to reproduce the general features and approximate magnitude of the $H^+ + H^-$ cross section, but differ from the ex-

perimental results in a number of significant details. Possible reasons for these discrepancies will be discussed later in this section.

Roy and Mukherjee [66] have performed a close coupled calculation on $H^+ + H^-$ over the lab energy range from 0.5 to 8 keV. The calculated cross section is in agreement with experiment at 8 keV, and is about 30% below experiment at 500 eV. This represents much better agreement at these high energies than any of the LZ calculations.

A particularly interesting feature of the experimental $H^+ + H^-$ results is the presence of some "fine structure" superimposed on the broad maximum around 300 eV. In addition to the two maxima and the minimum clearly indicated by the results, the scatter in the data between 30 and 100 eV indicates that there could be additional structure. Three extrema are observed that are roughly evenly spaced in reciprocal velocity, and may [32] be similar in origin to the oscillations seen in other cases of charge transfer or energy transfer. Another possible source of this structure is the variation of interaction energies with internuclear separation. Bates [58] and Mordinov and Firsov [67] have shown that the inclusion of this effect in an LZ calculation can possibly lead to two maxima in the cross section.

4.2. $N^+ + O^-$, $O^+ + O^-$

The experimental data on $N^+ + O^-$ of Aberth and Peterson [35], grouped according to energy, averaged and converted to cross sections, are presented in fig. 7.

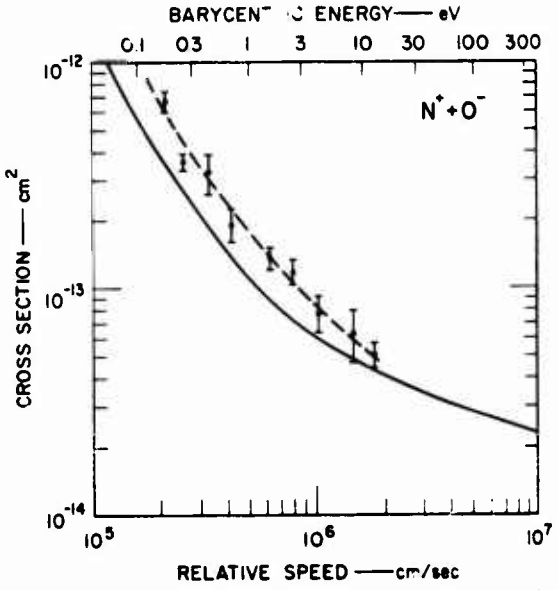

Fig. 7. Experimental [35] and theoretical [40] results for $N^+ + O^-$.

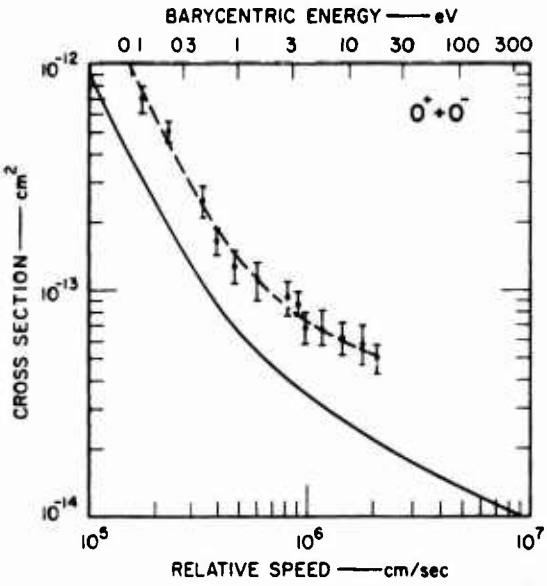

Fig. 8. Experimental [38] and theoretical [40] results for $O^+ + O^-$.

along with LZ calculation of Olson et al. [40]. This calculation is substantially more complicated than the $H^+ + H^-$ case since a large number of favorable crossings exist, and it is necessary to include ten excited N states, eight excited O states, and one state with excitation of both N and O. The calculations are further complicated by the fact that $N^+ + O^-$ may form six molecular states, requiring calculation of six sets of cross sections weighted by the appropriate statistical weight factor, and then summed. Details of the calculation, including matrix elements, crossing distances and energy differences for all states considered, are given in ref. [40]. It can be seen from fig. 6 that below 10 eV the theoretical results are slightly lower than the experimental values, but the energy dependence of the cross sections is well reproduced.

The system $O^+ + O^-$ has also been studied by the SRI group [38]. The results, shown in fig. 8 are seen to be very similar to the $N^+ + O^-$ results. The LZ calculations [40] are somewhat simpler since only six states need be considered; again the theoretical results are lower than the experimental values.

4.3. $He^+ + H^-$, $He^+ + D^-$

Gaily and Harrison [48] have investigated $He^+ + H^-$ over the energy range from 0.2 to 8 keV, with the results given by the triangles in fig. 9. The SRI group has made a limited number of measurements on $He^+ + D^-$ [40], represented by the circles. At relative velocities above 5×10^6 cm/sec the two cross sections should

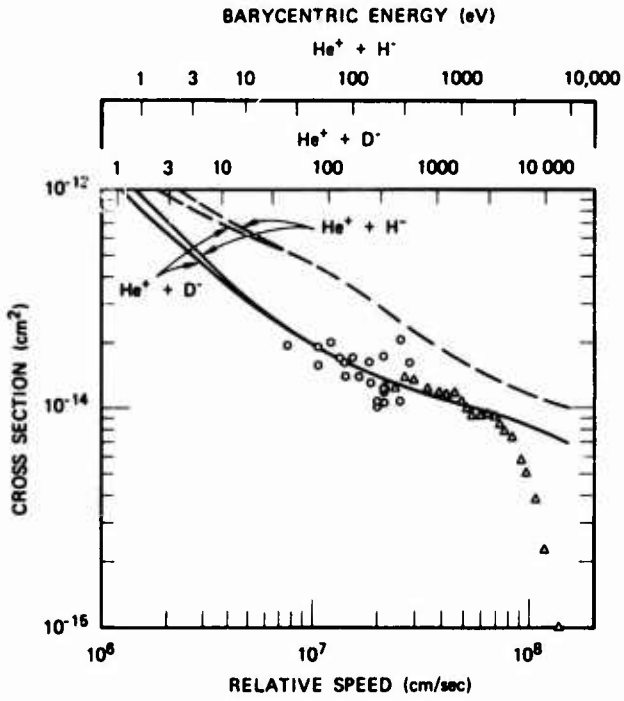

Fig. 9. Experimental results on $He^+ + H^-$ [48] (Δ) and $He^+ + D^-$ [40] (○), and theoretical results for both systems [40] using semi-empirical matrix elements (dashed lines) and the Smirnov formula [54] (solid lines).

be equal. The agreement, as evidenced by fig. 9, is satisfactory. Measurement at lower energies were not made because at the time these measurements were made the SRI merged beam apparatus was unable to merge ions of mass ratio 2 at very low relative energies. This limitation has since been removed [38].

The LZ calculations of Olson et al. [40] are also shown in fig. 9. Here, the dashed lines correspond to the matrix elements calculated by the Smirnov formula and the solid lines refer to matrix elements estimated by the semiempirical formula [54]. The discrepancy in energy dependence above 5 keV can again be explained by the invalidity of the LZ theory at these high energies. At low energies the cross section calculations predict the isotope (mass) effect mentioned in section 3.

The structure in the $He^+ + H^-$ measurements is actually more pronounced than it appears in fig. 9. This structure occurs in the same velocity range as the structure in the $H^+ + H^-$ cross sections, and most likely has the same origin.

4.4. $Na^+ + O^-$

The reaction $Na^+ + O^- \rightarrow Na + O$ was first studied by Weiner, Peatman and Berry [43,44], who observed photons emitted by the Na products, as described above in

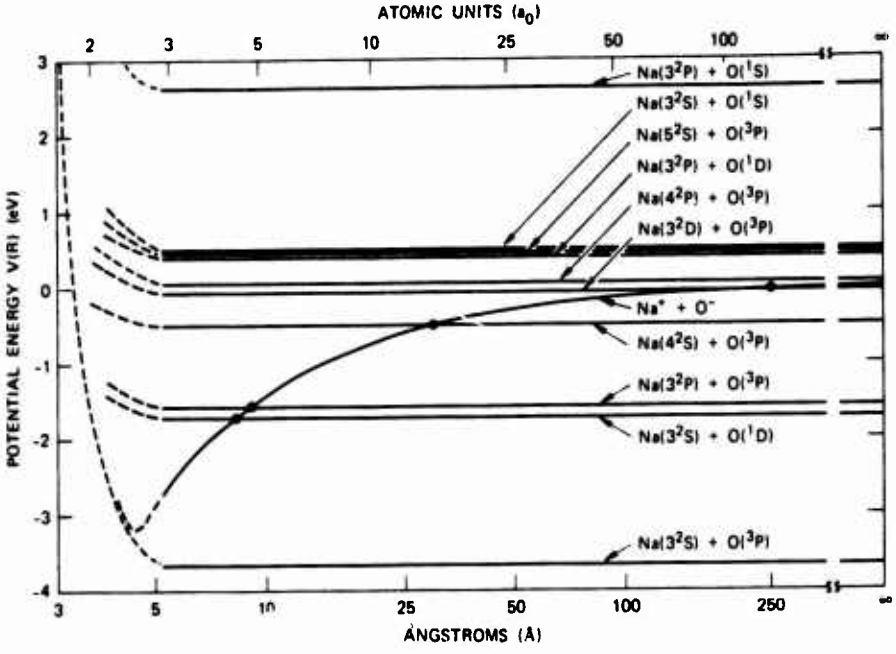

Fig. 10. Zero order potential curves for $Na^+ + O^- \rightarrow Na + O$.

section 2.2. The zero order potential curves for this system are presented in fig. 10. Measurements were made on photons from the Na $3^2D \rightarrow 3^2P$, 3^2S, and $4^2P \rightarrow 3^2S$ radiative transitions. The cross sections obtained from the $3^2D \rightarrow 3^2P$ transitions are shown in fig. 11. They are the largest yet reported for a mutual neutralization reaction. These results were suprising because the $Na^+ + O^-$ Coulomb potential crosses the $Na(3^2D) + O(^3P)$ curve at $R > 200$ Å and the LZ theory, using the semi-empirical matrix elements [54], predicts a negligibly small cross section for a curve crossing at such a large internuclear separation. Even more surprising from the curve-crossing viewpoint is the observation of a cross section of about 100 Å for the production of $Na(4^2P)$, for which the reaction is 0.1 eV endothermic. Such an endothermic reaction could depend on a curve crossing with the repulsive portion of the Coulomb potential at $R \lesssim 3$ Å, but this cross section would have an upper limit of less than πR^2, or about 30 Å^2.

The cross section obtained by observing the $3P \rightarrow 3S$ transition should be greater than that for the $3D \rightarrow 3P$, since it will include all the $3D \rightarrow 3P$ cascade contributions plus any direct contribution from the $Na(3P) + O(^3P)$ crossing at $\sim 17a_0$. In addition, it should be less than the total neutralization cross section since it will not in-

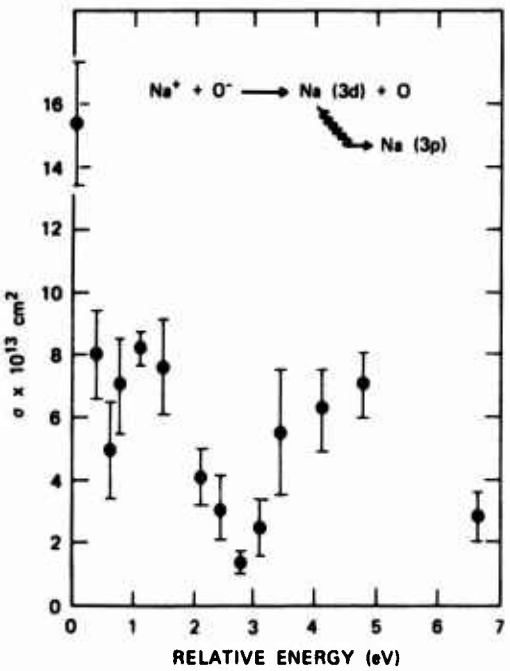

Fig. 11. Experimental results obtained from observation of the Na $3^2D \rightarrow 3^2P$ transition [44].

clude contributions from the observed $4P \rightarrow 3S$ transition, or from the Na(3S) + $O(^1D)$ crossing at $\sim 16a_0$.

The total cross section has been measured by the SRI group [38], and is shown on fig. 12, along with the $3P \rightarrow 3S$ results of Weiner et al. and a Landau–Zener calculation performed by Olson [68]. The SRI total cross section measurements are believed to be accurate to within ± 30%, and the absolute uncertainty in the 3P-3S measurements is placed at a factor of 2. The $3P \rightarrow 3S$ cross section are about three times larger than the total cross sections; thus even considering these error limits a discrepancy exists between the two measurements.

The magnitude of the $3P \rightarrow 3S$ cross section is also inconsistent with that of the $3D \rightarrow 3P$ cross section. Rather than being larger, it is in general smaller, and at 5 eV is about a factor of three smaller.

As we have discussed earlier, determination of absolute cross sections by this optical technique is quite difficult, and perhaps this inconsistency arises from a calibration error. In any case, it is our belief that the total cross section measurements of the SRI group give a more reliable result for the absolute magnitude of these cross sections. Nonetheless, the photon measurements of Weiner et al. are of considerable importance, since even if the actual $3D \rightarrow 3P$ cross section is an order of magnitude

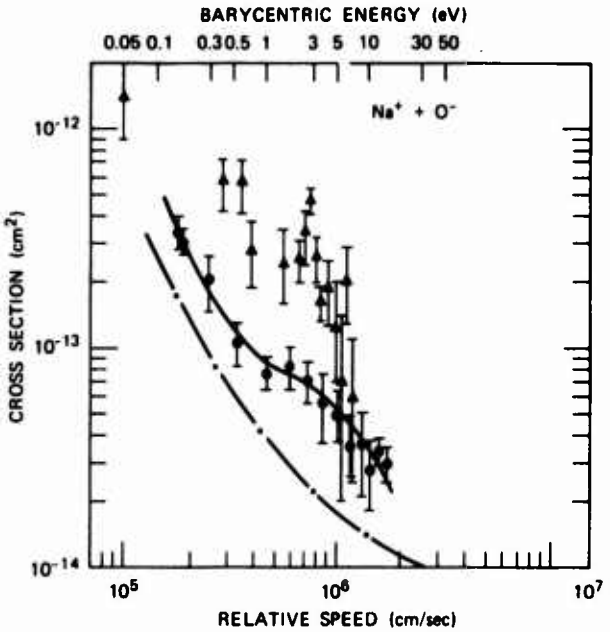

Fig. 12. Results for the total cross section $Na^+ + O^- \rightarrow Na + O$ [38] (●), from observation of the Na $3^2P \rightarrow 3^2S$ transition [44] (▲), and from a LZ calculation [68] (dot–dash line).

smaller than reported, the validitv of the simple LZ theory to predict product states is made questionable. Further investigations of emitted photons should shed considerable light on the mechanism of ion–ion interactions.

The results of the $Na^+ + O^-$ measurements encourages a more detailed consideration of the final states of the reaction than was presented in the discussion of the simple LZ theory in section 3. That discussion included only states that interact on the descending part of the Coulomb curve. Collision channels that remain on the Coulomb curve and reach the repulsive wall of the potential at $R \approx 3$ Å can also be considered. Interactions of the $Na(4^2P) + O(^3P)$ states are then not only possible but should be expected. Oscillations such as those observed on the cross sections for $Na(3^2D)$ and $Na(3^2P)$, which are roughly spaced as $1/v$ and are out of phase with one another, can result from transitions from the initial Colomb state to intermediate states that are mixed at larger separations at an avoided curve crossing via the Rosenthal mechanism [69]. However, calculations based on this model [68] of reaction on the repulsive wall of the interaction potentials yield cross sections about an order of magnitude smaller than those reported by Weiner et al.

Table 1
Reaction rate coefficients at 300 K — atomic ions. $\alpha(300\ \mathrm{K})$ — 10^{-7} cm^3/sec

System	Experimental	Theoretical
$H^+ + H^-$	3.9 ± 2.1	1.5[a]
		4.0[b]
		1.2 [51]
$N^+ + O^-$	2.6 ± 0.8	1.8[a]
$O^+ + O^-$	2.7 ± 1.3	1.1[a]
		~0.8 [50][c]
$Na^+ + O^-$	2.1 ± 1.0	0.7[b]
$He^+ + H^-$	—	5.7[a]
		7.3[b]
$He^+ + D^-$	—	4.7[a]
		5.7[b]

[a] Total cross sections calculated using eq. (26).
[b] Total cross sections calculated using eq. (27).
[c] It should be noted that the electronegativity of O used in this ref. [50] was 2.2 eV, whereas the value now accepted is 1.47 eV. Use of this value might substantially affect the calculated rate constant.

4.5. Thermal energy reaction rate coefficients

A primary interest in the ion–ion neutralization reaction is its importance in ionized gases. For such applications the parameter of importance is the reaction rate coefficient α at thermal temperatures. This rate can be estimated from the SRI data in the manner discussed below.

As discussed in section 3, the LZ formula can be approximated at low energies by the expansion

$$Q = A/v_r^2 + B/v_r + C + Dv_r. \tag{32}$$

Experimental data can be easily fit to such parameterization, and extrapolated to lower energies. The low-energy temperature dependence of the thermal rate coefficient $\alpha = \langle Qv_r \rangle$ can then be calculated [38] by Boltzmann averaging $v_r Q$. Error limits on α can be obtained from the uncertainty in the fitted curve and in the data. The dashed curves through the data in figs. 7 and 8 represent such parameterizations.

Table 1 gives reaction rates at 300°K for $H^+ + H^-$, $N^+ + O^-$, $O^+ + O^-$, and $Na^+ + O^-$ as determined from the data presented here. In addition, theoretical LZ values of α are given for these systems and for $He^+ + H^-$ and $He^+ + D^-$.

4.6. Discussion

From the measurements and calculations presented here, a number of generalizations can be made about atomic ion–ion mutual neutralization. Reaction rates at

thermal energies for such systems can be expected to exceed 10^{-7} cm^3/sec. The cross section at energies below a few tenths of an eV can be expected to vary essentially as $1/E$. Cross sections calculated using the LZ theory are usually smaller than are observed experimentally, but are within a factor of 2 or 3 of the measured cross sections, and they predict the general velocity dependence of the cross sections at low to intermediate velocities.

The general tendency of the LZ calculations to be somewhat smaller than experimental results could arise from a number of factors. The ions produced in the laboratory might not all be in their ground states, and hence a coupling to more states could result, giving rise to a large cross section. The LZ theory may not properly account for the range of R over which an interaction can occur. Further, the LZ theory clearly does not allow significant interaction at large or small distances, but both regions may be important. Evidence for this is found in the observation of Weiner et al. of large cross sections for the $Na^+ + O^-$ (3D → 3P) transition, even though the crossing is at nearly 300 Å, and for the 4P → 3S transition, even though no crossing occurs with the Na(4P) state until the repulsive part of the potential is reached. Similar interactions might account for most of the discrepancies between theory and experiment noted in this section. For example, the failure at low energies of the most rigorous calculations of $H^+ + H^-$ (curve b of fig. 5) may be due to the failure of the LZ formalism to properly account for the crossing at large distances to the $n = 4$ levels of hydrogen. More theoretical work is needed to understand the importance of transitions between curves which are nearly degenerate over long distances and to investigate the importance of close encounters. Additional experimental measurements of the final states of the resulting neutrals are also needed to verify the theoretical work.

5. Cross section calculations for molecular systems

It becomes very difficult to apply the LZ method presented in section 3 to the system

$$A^+ + B^- \rightarrow A + B + \Delta E \qquad (1)$$

when A or B or both are molecules. Now, the number of curve-crossings with the reactant Coulomb potential can easily reach into the hundreds due to the large number of excited electronic states and vibrational levels available. Even if the coupling matrix elements could be evaluated at each curve crossing, the computer time needed to solve for the transition probabilities via the simple LZ method becomes prohibitive. Therefore, some other approach must be used.

One reasonable assumption is that for the more complicated systems the physical situation may be approximated using a high density of crossing states. Then by using the Landau–Zener method and semi-empirical coupling matrix elements, a

critical crossing distance R_c can be calculated by assuming an absorbing-sphere model, i.e., unit probability exists for reaction within R_c. This approach is discussed in detail in ref. [42], and will be summarized here. To determine the critical distance R_c within which there is reaction, consider the application of the two-channel Landau–Zener method discussed in section 3. In this approximation the total cross section is given by eq. (28) where for the special case of thermal energy, λ, from eq. (30), approaches a constant given by $\sqrt{2}\pi R_x^{5/2}\mu^{1/2}H_{12}^2(R_x)$. In the two-channel case, the integral of the transition probabilities, $F_3(\lambda)$, eq. (29), has a maximum value of 0.113 when $\lambda = 0.424$.

If we now extend these results to the multichannel case where a large number of final states are available, we may expect reactions for all trajectories that approach within some critical internuclear separation R_c. Using the two-channel case as a guide, R_c will be slightly larger than the R value that satisfies $\lambda = 0.424$. The total cross section from eq. (28) will then be

$$Q = \pi R_c^2[1 + (R_c E)^{-1}]. \tag{35}$$

To determine λ, we must know its dependence on R. The coupling matrix element H_{12} is the only unknown, and from previous work on one-electron transfer, we have been able to parameterize it in terms of the effective ionization potential of the reactants and products. The relation was given in eq. (26) of section 3. This functional form for $H_{12}(R_x)$ is valid only at large distances, $R \gtrsim 10a_0$, where the electron is transferred through the potential barrier determined by the exponential tails of the wave functions for the reactant and product states and for values of I_i and I_f greater than ~ 0.4 eV.

By knowing the electron detachment energy of the negative ion and assuming that there is a high density of final states available for reactions, we may determine γ as a function of R using the relationship

$$I_f = I_i + R^{-1}. \tag{36}$$

Using eq. (26), it is an easy matter to obtain λ, eq. (30), as a function of R. From numerical calculations that include large numbers of final states, we find that λ approaches 0.15 as the density of the states approaches a continuum. The value $\lambda = 0.424$, which is correct for the two-channel case, tends to underestimate the cross section by about 10%. The use of $\lambda = 0.15$ to determine R_c has also been verified by Landau–Zener calculations employing a large number of product channels.

Because of the Coulomb attraction, the product EQ approaches a constant at very low (i.e. thermal) energies in eq. (35), so that the reaction rate α, which is an average over a Maxwellian distribution of ion velocities, becomes

$$\alpha = 4\pi\left(\frac{\mu}{2\pi kT}\right)^{3/2}\int_0^\infty Q\exp\left(\frac{-\mu v^2}{2kT}\right)v^3\,dv \approx 2(v^2Q)\left(\frac{\mu}{2\pi kT}\right)^{1/2}. \tag{37}$$

For molecular systems, the coupling matrix elements, eq. (26), should be modified by the Franck–Condon factors q that represent the overlap of the vibrational energy levels, to read [50]

$$H_{12}^{*} = q^{1/2} R^{*} \exp(-0.86R^{*}) . \tag{38}$$

The Franck–Condon factors are quantities less than unity so not including them in the calculation should provide an upper limit on the cross section. However, for the cases studied, even if all q_n were set equal to 0.1, the cross sections would be decreased by only about 20%. Therefore the results are not strongly affected by ignoring the Franck–Condon factors.

The simplified treatment above considers cases when a high density of final states exists in the region of most favorable curve crossings. Cross sections from these formulae thus represent upper limits to the actual values. On the other hand cross sections calculated in this manner are probably not much larger than the actual values even when the density of final states is low, since each reaction channel can then have a relatively high probability due to the lack of competition with neighboring channels. When the number of reactant states is large ($n \gtrsim 10$), the cross section is not strongly dependent on the number of states. The cross section is then found to approach closely the absorbing sphere value.

In the absorbing-sphere model described, the cross section is dependent only on the value of the electron detachment energy of the negative ion and the reduced mass of the system. A similar result is obtained in the work of Radtsig and Smirnov [70] who use a different approach to this problem.

In a given system, as the electron detachment energy is decreased because of vibrational or electronic excitation, the reaction rate increases. Physically, this corresponds to the outer electron on the negative ion being more loosely bound, making it possible for transfer to occur at larger intermolecular separations. If the negative ion is in an excited electronic or vibrational state, we would predict that the reaction rate will generally be greater than when the negative ion is in its ground state. This problem usually arises with molecular negative ions, but may also occur with an atomic negative ion system if the negative ion has a metastable electronic state.

In order to account for transitions that occur in a range around R_x, the Landau–Zener transition probabilities can be compared with the close-coupled values tabulated in reduced form by Delos [71]. It is found that the cross sections obtained by the Landau–Zener method are below the close-coupled results by approximately 10%. This factor is included in the absorbing sphere calculations to be presented here.

The energy dependence of the cross sections may be calculated using eq. (30) for the evaluation of λ. In fig. 13 are shown the cross section curves predicted by the absorbing sphere model for the negative ions studied here. The curves for each system are essentially independent (within 10%) of the positive ion mass when it is within a factor 2 of that of the negative ion.

As expected, the system with the lowest electron affinity, O_2, has the largest cross section at a given energy. Likewise, the system with the largest electron affinity, NO_3, has the smallest cross section. If the negative ion is in an excited level above its ground state, we would expect the observed cross sections to be larger than those predicted here.

A few comments should be made concerning the significance of the dissociation reaction

$$A^- + BC^+ \rightarrow A + B + C + \Delta E \tag{39}$$

since this may be the source of some of the theoretical and experimental differences in the molecular systems. Bates and Boyd [52] have presented Landau–Zener formulas for this process, and we find that the absorbing sphere model will be equally applicable to this type of reaction. The only difference between the theory for reaction (1) and that for reaction (39) is in the energy dependence of the cross sections. At low energies, in the region of practical interest for reaction rates, both reactions (1) and (39) will have a cross section that varies approximately as E^{-1}. At higher energies, the cross sections for reaction (1) continue to decrease, but at a rate slower than E^{-1}, until energies above about 1 keV are reached, when the dependence again approaches E^{-1}. The cross sections for reaction (39) at high energies, however, approach a constant value.

The cross section behavior at high energies therefore will depend on whether or not there are dissociating product channels available for reaction. We may predict

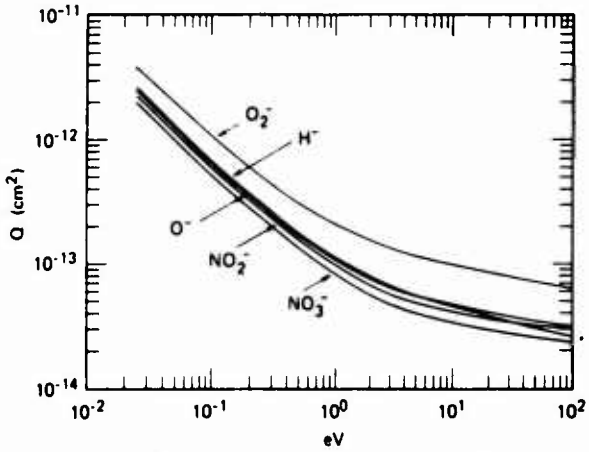

Fig. 13. Ion–ion mutual neutralization cross sections calculated using the absorbing sphere model [42]. In this model the cross section has only a very weak dependence on the mass of the positive ion.

that reaction (39) will be important when neutral states of the positive molecular ion have curve crossings in the important $R \approx 10$–$50a_0$ region, which lead to dissociation. These conditions will occur for dissociated neutral states that lie below the ground ion state by about 0.5 to 3.0 eV, plus the electron detachment energy of the negative ion. So far, the energy dependence of the experimental data on the molecular ions tends to indicate that the dissociation reaction is not a dominant process for those systems measured.

With regard to the vibrational effects in molecular ions, the most favored electronic transitions (which occur at large distances) will be to states with the greatest Franck–Condon factors. The extent to which vibrational energy is changed during the collision thus depends largely on the shapes and portions of the potential energy curves of the incident ions and product neutrals. It is reasonable to expect that some vibrational excitation is present in most bound product molecules.

Probably the most significant factor to note concerning the absorbing sphere model is the large reaction rate dependence on the electron detachment energy. If the electron detachment energy is decreased because of populated excited states of the negative ion, the cross sections increase. If the excitation is to the upper levels, this increase becomes significant. For upper atmosphere chemistry, this fact makes it desirable to know the excited state populations of the reactants for the ion–ion recombination reaction.

6. Simple molecular systems

6.1. $H_3^+ + D^-$

The $H_3^+ + D^-$ reaction represents a simple molecular ion system and consequently provides an important test for any theory describing neutralization reaction involving molecular ions. The results of measurements on this system [72] are given in fig. 14. The solid curve represents an absorbing sphere calculation [68]. There is apparently some oscillatory structure in the experimental data above 5 eV, although the magnitude of the errors casts some doubt on this conclusion. The absorbing sphere calculation of the rate coefficient at 300° K yields the value of (8.5 ± 1.5).* Extrapolation of the experimental results yields (4.7 ± 1.5).

6.2. $NO^+ + O^-$, $O_2^+ + O^-$

Results for the reactions $NO^+ + O^-$ and $O_2^+ + O^-$ [38] are given in figs. 15 and 16. The data here are plotted as the product of the relative velocity v_r and the cross section Q. This product is effectively a mono-energetic reaction rate. The energy dependence of these rates are typical for ion–ion neutralization involving complex ions. The solid curves in the figures represent a least-squares fit of the data to the functional form of eq. (32).

* All rate coefficients will be expressed in the units 10^{-7} cm^3/sec, and these units will be omitted in the text.

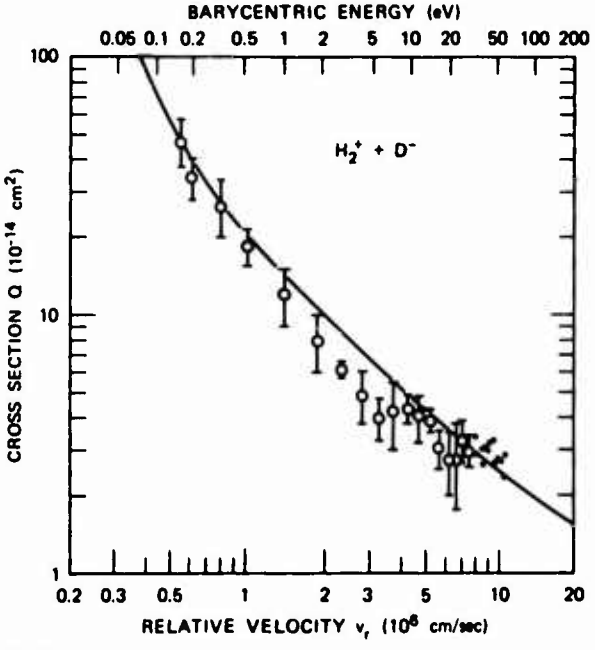

Fig. 14. Experimental [72] and theoretical [68] results on $H_2^+ + D^-$.

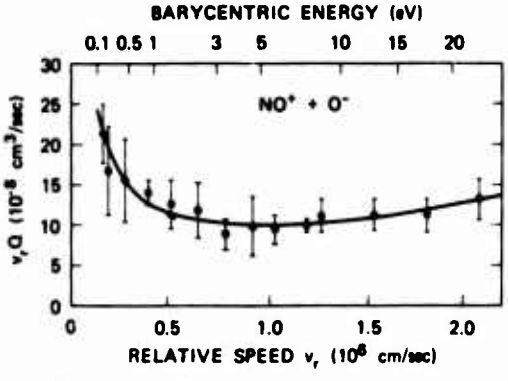

Fig. 15. Experimental results [38] on $NO^+ + O^-$.

It is interesting to compare these reactions with the atomic ion reactions that have been investigated for O^-. Fig. 17 shows the cross sections for all five positive ions that have been studied with O^-. All of the reactions show a very similar energy dependence, and, except for NO^+, have very nearly the same magnitude.

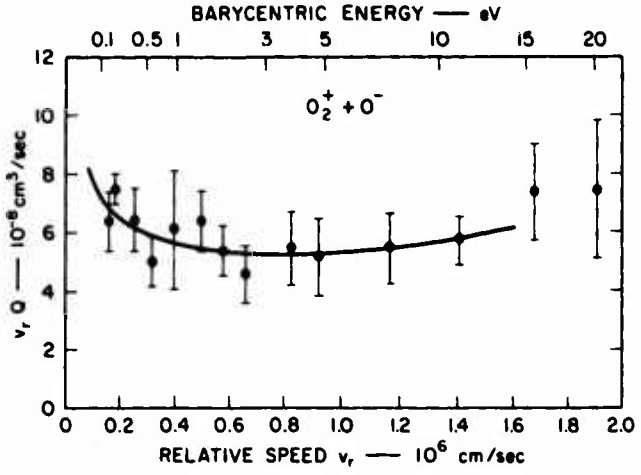

Fig. 16. Experimental results [38] on $O_2^+ + O^-$.

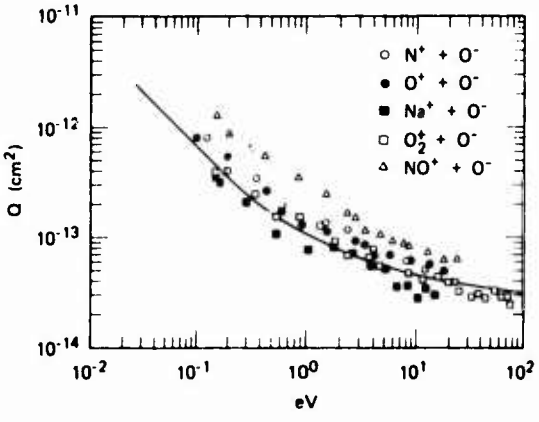

Fig. 17. Results for the neutralization of N^+, O^+, Na^+, O_2^+, and NO^+ by O^-. The solid curve is from an absorbing sphere calculation [42].

The solid curve represents an absorbing sphere calculation by Olson [42]. As has been discussed, for this model the cross section is dependent only on the value of the electron detachment energy of the negative ion and the reduced mass of the system. It is striking that such a simple model yields quite good agreement with the experimental results, and that in fact the cross sections, except for NO^+, are very nearly equal.

The experimental cross sections were extrapolated to lower energies, and the reaction rates at 300° K were calculated in the manner described earlier. The results, for NO^+ and O_2^+ respectively, were (4.9 ± 2.0) and (1.0 ± 0.4). Absorbing sphere calculations predict (1.9 ± 0.6) for both of these reactions.

6.3. $I_2^+ + I^-$

Recombination for iodine ions formed in a gas has been studied at temperatures near 300° K. Yeung [1] observed the change in the dielectric constant in iodine vapor due to the decay of ions following a discharge. Greaves [25] used the same technique, but added a mass spectrometer to identify the ions present. He also corrected a calibration error in Yeung's experiment which had caused Yeung's reported values to be too small by a factor of 10. Carlton and Mahan [28] formed ions by photo-ionization and used charge collection to monitor the decay of the ion concentration. The values obtained for α at room temperature by these three experiments are, respectively, (1.47 ± 0.07), (1.22 ± 0.03) and (1.45 ± 0.5). Although the first two values do not agree within the quoted errors, the overall agreement for these three experiments is quite good. However, it has been pointed out [21] that the condition that diffusion effects be negligible is only marginally satisfied by all of these experiments, and as a result, each of these results may be high by as much as 20 to 30%.

Yeung and Greaves investigated the temperature dependence of the $I_2^+ + I^-$ reaction. The recombination rate was observed to decrease with increasing temperature, as expected. Although the temperature range was quite limited, both results appear to indicate a decrease in the cross section substantially faster than the expected $1/E$ (or $1/T$) dependence.

7. Complex molecular systems

Recombination systems in which both positive and negative ions are molecular are quite complex since a large number of potential surfaces will be involved in the

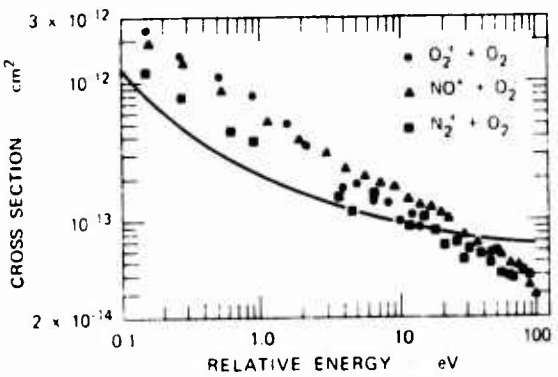

Fig. 18. Results for the neutralization of O_2^+, NO^+, and N_2^+ by O_2. The solid curve is from an absorbing sphere calculation [68].

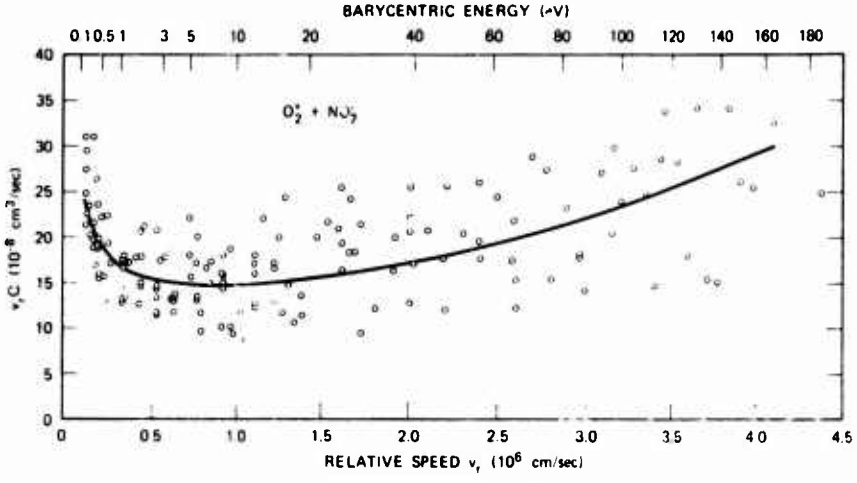

Fig. 19. Experimental results [39] on $O_2^+ + NO_2^-$.

reaction. Very little is known about most of these potentials, and a wide variety of final states, both dissociating and non-dissociating, are likely to be involved. It is ions of this type, however, that are responsible for the behavior of most ionized gases of practical importance. We shall discuss reactions that are grouped according to the negative incident ion.

7.1. Neutralization with O_2^-

Measurements have been made on the neutralization of O_2^- with N_2^+ [35], O_2^+ [39], and NO^+ [73]. The results are shown in fig. 18. The solid curve is from an absorbing sphere calculation [68]. The NO^+ and O_2^+ cross sections are very nearly equal, while the N_2^+ cross section is smaller, particularly at lower energies.

Extrapolation of the higher energy $O_2^+ + O_2^-$ results shown in fig. 18 yields (4.2 ± 1.3) and an absorbing sphere calculation yields (2.4 ± 0.8). A measurement of the $O_2^+ + O_2^-$ neutralization rate at thermal energy has been reported by Hirsh and Eisner [74]. They obtained a value of (1.0 ± 0.1). Possible reasons for those differences will be discussed later in this section.

7.2. Neutralization with NO_2^-

Neutralization rates have been measured for $O_2^+ + NO_2^-$ and $NO^+ + NO_2^-$ [39] over the energy range from 0.15 to 200 eV and are shown in figs. 19 and 20. The rates and energy dependencies of these two reactions are quite different at energies above 5 eV, but below this energy the rates are nearly equal. Extrapolation of these results yields a rate at 300° K of (4.1 ± 1.3) for O_2^+ and (5.1 ± 1.5) for NO^+. Very recent measurements at SRI, as yet unpublished, yield a 300° K rate for $N_2^+ + NO_2^-$ of (1.3 ± 0.5).

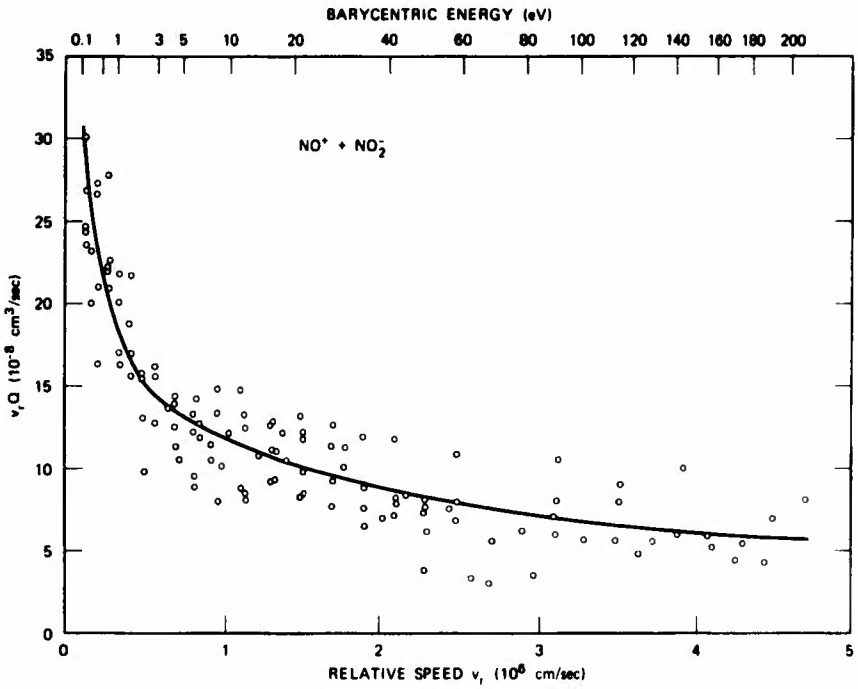

Fig. 20. Experimental results [39] on $NO^+ + NO_2^-$.

A thermal energy (300° K) rate of (1.75 ± 0.6) has been measured for $NO^+ + NO_2^-$ by Eisner and Hirsh [26]. Mahan and Person [27] have reported a rate of (2.1 ± 0.6) for ions believed to be primarily NO^+ and NO_2^-. Absorbing sphere calculations yield (1.2 ± 0.3) for both O_2^+ and NO^+, and (1.3 ± 0.3) for N_2^+.

7.3. *Neutralization with* NO_3^-

Eisner and Hirsh [26] have reported a thermal rate of (0.34 ± 0.12) for $NO^+ + NO_3^-$. This is the smallest value for a thermal energy rate that has been reported. Absorbing sphere calculations yield a value of (1.1 ± 0.3), and merged beam measurements [72] yield a value of 3 at 0.15 eV, and extrapolate to (8.1 ± 2.3) at thermal energy. Clearly there is a substantial discrepancy in these values.

The merged beam measurements on NO_3^- are subject to some important uncertainties that are not present in measurements on other ions. First, the NO_3^- beam may have been contaminated with some NO_2^- ions. In order to merge NO^+ and NO_3^- at low relative energy, it was necessary to bring the negative ion beam into the merging magnet near its centerline. This reduced the total mass resolution of the system to a point where NO_2^-, which is formed by the source in much greater abundance than NO_3^-, may have been present along the interaction length. Second, since the NO_3^- current was small, the resulting neutral signal was small, and it is pos-

sible that the preamplifier stage of the lock-in amplifier was overloaded by the non-coherent, background neutrals. Third, the ion NO_3^- exists in two distinct forms which have quite different electron affinities [75]. The NO_3^- ions used in the merged beam were formed in a mixture of NO and O_2, and might therefore consist primarily of the lower electron affinity "peroxy" form ($NO \cdot O_2^-$) which is believed to have a linear configuration. The NO_3^- ions of Eisner and Hirsh were formed in an airlike N_2: O_2 mixture, and might consist primarily of the "normal" nitrate form of NO_3^-. These two forms of NO_3^- would be expected to have different neutralization rates, but not so different as the results of these two measurements. A fourth uncertainty, which stems from possible vibrational or electronic excitation of the ions, is common to all measurements using molecular beams, and will be discussed later.

The $O_2^+ + NO_3^-$ reaction has also been investigated using the merged beam apparatus. This measurement was subject to the same uncertainties as the $NO^+ + NO_3^-$ measurement, but it yielded substantially different results. The mono-energetic rate was very nearly constant from 0.15 to 700 eV at a value of 1.2, and the extrapolation yielded a thermal energy rate of (1.3 ± 0.4). An absorbing sphere calculation yielded (1.0 ± 0.2).

7.4. Discussion of molecular ion reactions

The thermal reaction rate coefficients obtained for all systems involving molecular ions are summarized in table 2. The theoretical results are all from absorbing sphere calculations. The agreement is generally within a factor of two for the O^- and O_2^- systems, however there are larger discrepancies between theory and experiment for $NO^+ + O^-$ and $NO^+ + O_2^-$ reactions and for most reactions involving NO_2^- and NO_3^-. In general, the result obtained by extrapolating the merged beam measurements are larger than the theoretical predictions, and the measurements of Eisner and Hirsh are lower.

It is possible that some of the merged beam cross sections are relatively large because of internal excitation in the incident ions. The ions in the two beams are formed in duoplasmatron ion sources and probably are vibrationally excited. In addition, if metastable electronic states exist they may also be populated. If present, both of these forms of excitation would tend to increase the neutralization cross sections, although the actual magnitude of the effect is unknown. Electronic excitation generally opens up more possible final states, and the general effect will be to increase the reaction cross sections. Vibrational excitation, on the other hand, has a more limited effect since it will increase the cross sections only when the effective vibrational overlap with the final states is increased by its presence.

From the observation that the rate for NO^+ and any negative ion were found to be the largest for that negative ion, it was speculated that the merged beam rates may have been increased by the presence of metastable NO^+ in the beam. The $A^2\Pi$ state of NO^+ is 6 eV above the ground state and could yield much larger cross sections, especially in the case of NO_3^-, which has a very high electron detachment en-

Table 2
Reaction rate coefficients at 300° K – molecular ions. $\alpha(300° K) - 10^{-7}$ cm^3/sec

System	Experimental[a]	Theoretical [42]
$H_2^+ + D^-$	4.7 ± 1.5	8.5 ± 2.1
$N_2^+ + O^-$	–	2.0 ± 0.6
$NO^+ + O^-$	4.9 ± 2.0	1.9 ± 0.6
$O_2^+ + O^-$	1.0 ± 0.4	1.9 ± 0.5
$N_2^+ + O_2^-$	1.6 ± 0.5	2.5 ± 0.8
$NO^+ + O_2^-$	5.8 ± 1.0	2.4 ± 0.8
$O_2^+ + O_2^-$	4.2 ± 1.3	2.4 ± 0.8
	1.0 ± 0.1 [74]	
$N_2^+ + NO_2^-$	1.3 ± 0.5	1.3 ± 0.3
$NO^+ + NO_2^-$	5.1 ± 1.5	1.2 ± 0.3
	2.1 ± 0.6 [27]	
	1.75 ± 0.6 [32]	
$O_2^+ + NO_2^-$	4.1 ± 1.3	1.2 ± 0.3
$NO^+ + NO_3^-$	8.1 ± 2.3	1.1 ± 0.3
	0.34 ± 0.12 [32]	
$O_2^+ + NO_3^-$	1.3 ± 0.4	1.0 ± 0.2

[a] Experimental results are from SRI merged beam measurements unless otherwise noted.

ergy. However, measurements at SRI [73] have shown that less than 10% of the NO^+ was electronically excited in the merged beam experiments. It is inconceivable that such a small excited fraction could increase the rates by enough to account for the observed differences.

For NO_3^-, it seems likely, as is mentioned in the previous section, that the merged beam measurements were made using the low electron affinity $NO \cdot O_2^-$ form of the ion. However, it is doubtful that any such excitation can account for more than a small fraction of the observed differences. For example, in the absorbing sphere model, decreasing the electron attachment energy from 3.6 to 2.5 eV increases the calculated thermal energy rate by only 10%. For NO_2^-, a decrease from 2.3 to 1.8 eV increases the rate by only 15%.

The extrapolation technique discussed earlier could lead to larger errors than expected. However, the $O_2^+ + NO_2^-$ and $NO^+ + NO_2^-$ rates have already reached 2.5×10^{-7} cm^3/sec at 0.15 eV and are clearly increasing rapidly at the low energy limit of the merged beam measurements. It is highly unlikely that the extrapolation technique could lead to errors larger than a factor of two in the thermal energy reaction rates.

Thus there are unresolved discrepancies between experiments and theory for rates involving NO_2^- and NO_3^-. By far the most serious discrepancy is for $NO^+ + NO_3^-$. Because of the importance of this reaction additional investigations are planned at SRI.

7.5. Hydrated ions

Although it is now known that under normal quiescent conditions the ions in the D-region are predominantly in hydrated forms as discussed briefly in section 1, no laboratory measurements have yet been made on any of these species. Early efforts at SRI were thwarted by the inability to produce the hydrated species in the duoplasmatron ion sources. The ions are formed in three-body reactions such as (7), and the conditions in conventional duoplasmatrons apparently either are too hot or too violent to allow production in sufficient quantities to be useful. Recent attempts at SRI, using a duodehcatron source [76] have been more successful, and there now is a good chance to perform measurements on at least some of the simpler hydrates.

As water molecules are attached to the negative ions, several effects tend to slow down the neutralization rate. Firstly, both of the parent ions will be somewhat shielded from each other by the water molecules, so that the electron transfer probability is reduced at each moment during the collision; secondly, the energy required to remove the electron from the negative ion is increased by about 1.2 eV per H_2O molecule, so that the number of neutral state crossings available to the reaction is decreased, further reducing the reaction cross section; thirdly, the increased mass reduces the average velocity at each temperature and the rate $\alpha = vQ$ is reduced even if the reaction cross section is unchanged.

On the other hand, another factor will tend to increase the rate. As these large molecules, which are usually polar or polarizable, come together under the influence of the Coulomb force, internal vibrational and rotational modes can be excited by the action of the electric field on the moving and rotating dipole. If the induced excitation energy in these modes exceeds kT, the ions will be trapped in a stable orbit, and many more curve crossing can occur to allow neutralization before the internal excitation can be removed and the participles fly apart. Or, additional internal modes may be excited to bind the molecules in even tighter orbits. For very large hydrated ions where the number of attached water molecules exceeds about 5 or more, the chance for orbital capture is very high but the probability of electron transfer may be very low, so that the ions many actually recombine into a large neutral water cluster bound together by the Coulomb attaction between the core ions. Some water molecules would "boil" off during the process, but the ions would still be isolated by the remaining water molecules.

These effects are now under theoretical study at SRI. Huestis, Smith and Benson have shown, in preliminary results, that induced rotational excitation can affect the rates even for a simple pair such as $O^- + NO^+$ [77]. These effects have not been included in any of the Landau–Zener or absorbing sphere calculations, and may account for some of the tendency for the theory to underestimate the reaction rates. The influence of internal mode excitation should be considerably greater for the hydrated ions than for the simpler ions that have been measured so far, thus the results of the present experiments and theoretical efforts should be very interesting.

8. Concluding remarks

A great deal of progress in understanding the ion–ion mutual neutralization reaction has been made in the last five years. The merged beam experiments have yielded data on a large number of reactions between atomic and simple molecular ions, over a large energy range, providing a very useful basis for the testing of theoretical calculations, as well as data from which could be obtained reaction rates that were previously unknown. These rates were primarily sought for use in ionospheric modeling, but they are also important for the understanding of flame and gas laser phenomena. A theory based on the Landau–Zener approach, using semiempirical interaction matrix elements, has been found to be reasonably good for the atomic species, although it cannot predict detailed structure such as found experimentally in the $H^+ + H^-$ case. In order to handle the more complicated problem of molecular ion reactions, the absorbing sphere model was developed and found to be useful for estimating unmeasured reaction rates between simple molecules. Thus the reaction is now reasonably well understood for atomic and simple molecular ions, as far as the total cross section or reaction rates are concerned.

The major remaining problem from the practical standpoint of the reaction rates needed for ionospheric applications is to determine the cross sections and rates for hydrated ion reactions. Both theoretical and experimental efforts are under way at SRI, aimed toward this problem. The theory has already pointed out the importance of the excitation of internal energy modes during the collision, which was not taken into account in the treatment of the simpler molecules.

Another outstanding problem is the determination of the final states and products of the reactions. Except for the optical measurements on $Na^+ + O^-$, there have been no attempts to study this aspect of ion–ion neutralization. Severe experimental difficulties are associated with the identification of the neutral product species for molecular systems, where dissociation is often likely to occur; consequently this remains as a major unknown in atmospheric modeling. Because of the experimental difficulties, it is likely that the best information on the reaction final states and product species for molecular reactant will be obtained theoretically. Present theories are inadequate for such detailed predictions. In order to develop adequate theories, more detailed experimental data are required, such as optical measurements of final states of reactions between atomic ions and some simple molecular systems.

Acknowledgments

The authors wish to thank Stanford Research Institute for its internal support of a major part of the effort that went into the preparation and writing of this review. We wish to thank Dr. Felix T. Smith for his encouragement and for his contributions to our understanding of the reaction mechanism. The research carried

out at SRI on this problem was supported by the Defense Nuclear Agency, through Air Force Cambridge Research Laboratory, and we wish to thank Drs. K.S.W. Champion and J.F. Paulson, of AFCRL, for their guidance on matters pertaining to the applications of our work to ionospheric problems.

References

[1] T.H.Y. Yeung, Proc. Phys. Soc. (London) 71 (1958) 341.
[2] P.F. Knewstubb and T.M. Sugden, Trans. Far. Soc. 54 (1958) 372.
[3] A.P. Mitra, J. Atmos. Terr. Phys. 10 (1957) 153.
[4] A. Dalgarno, Ann. Geophys. 17 (1961) 16.
[5] M.A. Biondi, Ann. Geophys. 20 (1964) 34.
[6] R.E. LeLevier and L.M. Branscomb, J. Geophys. Res. 73 (1968) 27.
[7] A.P. Mitra, J. Atmos. Terr. Phys. 30 (1968) 1065.
[8] D.R. Bates, Contemp. Phys. 11 (1970) 105.
[9] R.S. Narcissi, Composition Studies of the Lower Ionosphere, in: Physics of the Upper Atmosphere, ed. F. Verniani (Typographia Compositori, Bologna, 1971) pp. 12–59.
[10] R.S. Narcissi, C.R. Philbrick, M.A. McLeod and N.W. Rosenberg, Trans. Am. Geophys. U. 53 (1972) 462.
[11] K.W. Berkner, R.V. Pyle and J.W. Stearns, Phys. Rev. 178 (1969) 248.
[12] B.J. Woodward, W.C. Lineberger and L.M. Branscomb, submitted to Phys. Rev. A; B.J. Woodward, Thesis, JILA Report No. 102, Univ. of Colorado (1970).
[13] G.A.L. Delvigne and J. Los, Physica 67 (1973) 166.
[14] D.R. Bates and H.S.W. Massey, Phil. Trans. Roy. Soc. A 239 (1943) 269.
[15] L. Landau, J. Phys. (USSR) 2 (1932) 46.
[16] C. Zener, Proc. Roy. Soc. (London) A 137 (1933) 696.
[17] E.C.G. Stückelberg, Helv. Phys. Acta 5 (1932) 369.
[18] J. Sayers, Ionic Recombination, in: Atomic and Molecular Processes, ed. D.R. Bates (Academic Press, New York, 1962) pp. 272–280.
[19] D.R. Bates, Comments on Atomic and Molecular Physics 2 (1970) 107.
[20] D.R. Bates, Recombination, in: Case Studies in Atomic Physics 4 (1974) 57.
[21] B.H. Mahan, Recombination of Gaseous Ions, in: Advances in Chemical Physics, eds. I. Prigogini and S.A. Rice (Wiley, New York, 1973) pp. 1–40.
[22] M.R. Flannery, Three-body Recombination of Positive and Negative Ions, in: Case Studies in Atomic Collision Physics, Vol. 2, eds. E.W. McDaniel and M.R.C. McDowell (North-Holland, Amsterdam, 1972) pp. 1–90.
[23] E.W. McDaniel, Collision Phenomena in Ionized Gases (Wiley, New York, 1964) Ch. 12.
[24] H.S.W. Massey, E.H.S. Burhop and H.B. Gilbody, Electronic and Ionic Impact Phenomena, Vol. 4 (Clarendon Press, Oxford, 1974).
[25] C. Greaves, J. Electron. Control 17 (1964) 171.
[26] P.M. Eisner and M.N. Hirsh, Phys. Rev. Letters 26 (1971) 874.
[27] B.H. Mahan and J.C. Person, J. Chem. Phys. 40 (1964) 392.
[28] T.S. Carlton and B.H. Mahan, J. Chem. Phys. 40 (1964) 3683.
[29] G.A. Fisk, B.H. Mahan and F.K. Parks, J. Chem. Phys. 47 (1967) 2649.
[30] S. McGowan, Can. J. Phys. 45 (1966) 429.
[31] S. McGowan, Can. J. Phys. 45 (1966) 439.
[32] M.N. Hirsh and P.N. Eisner, Radio Sci. 7 (1972) 125.
[33] F.G. Niles, private communication.
[34] W. Aberth, J.R. Peterson, D.C. Lorents and C.J. Cook, Phys. Rev. Letters 20 (1968) 979.

[35] W. Aberth and J.R. Peterson, Phys. Rev. A 1 (1970) 158.
[36] R.H. Neynaber, Experiments with Merging Beams, in: Advances in Atomic and Molecular Physics, Vol. 5, eds. D. Bates and I. Esterman (Academic Press, New York, 1969) pp. 57–108.
[37] J. Moseley, W. Aberth and J.R. Peterson, Phys. Rev. Letters 24 (1970) 435.
[38] J.T. Moseley, W. Aberth and J.R. Peterson, J. Geophys. Res. 77 (1972) 255.
[39] J.R. Peterson, W. Aberth, J.T. Moseley and J.R. Sheridan, Phys. Rev. A 3 (1971) 1651.
[40] R.E. Olson, J.R. Peterson and J.T. Moseley, J. Chem. Phys. 53 (1970) 3391.
[41] R.E. Olson, J.R. Peterson and J. Moseley, J. Geophys. Res. 76 (1971) 2516.
[42] R.E. Olson, J. Chem. Phys. 56 (1972) 2979.
[43] J. Weiner, W.B. Peatman and R.S. Berry, Phys. Rev. Letters 25 (1970) 79.
[44] J. Weiner, W.B. Peatman and R.S. Berry, Phys. Rev. 4 (1971) 1825.
[45] L. Birenbaum and D.B. Searl, Appl. Optics 12 (1973) 519.
[46] R.D. Rundel, R.L. Aitken and M.F.A. Harrison, J. Phys. B 2 (1969) 954.
[47] T.D. Gailey and M.F.A. Harrison, J. Phys. B 3 (1970) L27.
[48] T.D. Gailey and M.F.A. Harrison, J. Phys. B 3 (1970) 1098.
[49] H.S.W. Massey, Negative Ions (2nd ed., Cambridge Press, 1950) p. 93.
[50] J.L. Magee, Disc. Faraday Soc. 12 (1952) 33.
[51] D.R. Bates and J.T. Lewis, Proc. Phys. Soc. (London) A 68 (1955) 173.
[52] D.R. Bates and T.J.M. Boyd, Proc. Phys. Soc. (London) A 69 (1956) 910.
[53] J. van den Bos, J. Chem. Phys. 52 (1970) 3254; 57 (1972) 3586.
[54] R.F. Olson, F.T. Smith and E. Bauer, Appl. Optics 10 (1971) 1848.
[55] E. Bauer, E.R. Fisher and F.R. Gilmore, J. Chem. Phys. 51 (1969) 4173.
[56] J.B. Hasted and A.Y.J. Chong, Proc. Phys. Soc. (London) 80 (1962) 441.
[57] B.M. Smirnov, Sov. Phys. Dokl. 10 (1965) 218; 12 (1967) 242.
[58] D.R. Bates, Proc. Roy. Soc. (London) A 257 (1960) 22.
[59] D.R. Bates, H.C. Johnston and I. Stewart, Proc. Phys. Soc. (London) 84 (1964) 517.
[60] G.V. Dubrowskii, Zh. Eksp. i Teor. Fiz. 46 (1964) 863; 47 (1964) 644.
[61] J.C. Browne and G.A. Victor, private communication.
[62] A. Dalgarno, G.A. Victor and P. Blanchard, Theoretical Studies of Atomic Transitions and Interatomic Interactions, AFCRL Report No. 71–0342.
[63] R.G. Gordon, J. Chem. Phys. 51 (1969) 14.
[64] D.R. Bates and D.S.F. Crothers, Proc. Roy. Soc. (London) A 315 (1970) 465.
[65] R.K. Janev and A.R. Tancic, J. Phys. B 5 (1972) L250.
[66] K. Roy and S.C. Mukherjee, Phys. Rev. A 7 (1973) 130.
[67] Y.P. Mordinov and O.B. Firsov, Zh. Eksp. i Teor. Fiz. 39 (1960) 427.
[68] R.E. Olson, private communication.
[69] H. Rosenthal, Phys. Rev. A 4 (1971) 1030.
[70] A.A. Radtsig and B.M. Smirnov, 7th Intern. Conf. on the Physics of Electronic and Atomic Collisions, Abstracts of Papers (North-Holland, Amsterdam, 1971) p. 481.
[71] J.B. Delos, Semiclassical Study of the Potential Crossing Problems in Atomic Collisions Theory, unpublished thesis, Massachusetts Institute of Technology, 1970.
[72] W. Aberth, J.T. Moseley and J.R. Peterson, Two Body Ion–Ion Neutralization Cross Sections, AFCRL Report No. 71-0481, Air Force Cambridge Research Laboratories, Bedford, Mass., 1971.
[73] J.T. Moseley and J.R. Peterson, Bull. Am. Phys. Soc. 17 (1972) 1136.
[74] M.N. Hirsh and P.N. Eisner, Bull. Am. Phys. Soc. 17 (1972) 395.
[75] F.F. Ferguson, D.B. Dunkin and F.L. Fehsenfeld, J. Chem. Phys. 57 (1972) 1459.
[76] G.M. Klody and H.T. Richards, Bull. Am. Phys. Soc. 15 (1970) 642; 17 (1972) 570.
[77] D.L. Huestis, F.T. Smith and S.W. Benson, Transactions, Am. Geophys. Union 54 (1973) 1099.